4C 41.17 - A radio galaxy at a redshift of 3.8

Chambers, K.C.; Miley, G.K.; Breugel, W.J.M. van

THE ASTROPHYSICAL JOURNAL, 363:21–39, 1990 November 1

4C 41.17: A RADIO GALAXY AT A REDSHIFT OF 3.8

K. C. CHAMBERS[1,2,3]
Space Telescope Science Institute; and Department of Physics and Astronomy, The Johns Hopkins University
G. K. MILEY[1,2,3]
Space Telescope Science Institute; and Sterrewacht, Leiden
AND
W. J. M. VAN BREUGEL[1,2]
Institute for Geophysics and Planetary Physics, Lawrence Livermore National Laboratory
Received 1990 January 8; accepted 1990 April 23

ABSTRACT

We report the discovery and study of the most distant radio galaxy observed to date. A multispectral investigation of the ultrasteep spectrum radio source 4C 41.17 has identified a faint extended optical/infrared counterpart whose spectrum shows two emission lines with wavelengths corresponding to those of Lyα and C IV λ1549, redshifted by $z = 3.800 \pm 0.003$. The extended optical continuum emission ($\sim$30 kpc) together with the large rest frame equivalent width of Lyα ($\sim$270 Å) indicate that 4C 41.17 is a distant radio galaxy.

The properties of the radio synchrotron emission, the optical/infrared continuum, and the line-emitting gas of 4C 41.17 are presented and discussed. The radio emission is dominated by compact ultrasteep spectrum emission with a spectral index ~ -1.3. As is the case with other high-redshift radio galaxies, the extended optical/infrared continuum is aligned with the radio axis. The rest frame spectral energy distribution (SED) exhibits a steep falloff shortward of Lyα, a possible "1500 Å break," a flat region in the ultraviolet, and a rise in the form of a "red bump" longward of $\sim$4000 Å.

Various mechanisms for producing the optical/IR emission in 4C 41.17 are considered in the light of the observed radio/optical alignment. It is concluded that a large fraction of the SED is probably from stars and that star formation induced by the radio source is the likeliest mechanism to account for the radio/optical alignment. For a normal IMF, stellar population models imply a total mass in stars of $\sim 5 \times 10^{11}\ M_\odot$ for $q_0 = 0.5$ to $\sim 25 \times 10^{11}\ M_\odot$ for $q_0 = 0$. Although the SED is consistent with emission from an old stellar population ($\sim 1.5 \times 10^9$ yr), this would make 4C 41.17 comparable with or older than the age of the universe for $H_0 = 50$, $q_0 = 0.5$, and create difficulties in explaining the optical/radio alignment. Alternatively, the SED can be produced by a galaxy whose age is as low as $\lesssim 3 \times 10^8$ yr, if most of the stars formed on time scales $\lesssim 10^8$ yr. This is comparable with the likely age of the radio source and is therefore consistent with a scenario in which the star formation is associated with the radio source.

The Lyα emission-line gas is elongated along the radio axis and includes an elliptical halo that extends more than 100 kpc, beyond the bright components of the radio source. The velocity field has a dispersion of $\sim$400 km s^{-1} but with a total amplitude as large as $\sim$2500 km s^{-1} in regions well correlated with the radio source. It is suggested that the kinematics of the high velocity gas is affected by entrainment in the radio jet. Various mechanisms for ionizing the extended gas are considered. At least two-thirds of the Lyα flux could be due to photoionization by stars responsible for the continuum emission. Other mechanisms which may contribute to the ionization are photoionization by photons emitted anisotropically along the radio axis and processes directly associated with the radio jet.

Subject headings: galaxies: evolution — galaxies: formation — galaxies: individual (4C 41.17) — galaxies: redshifts — radiation mechanisms — radio sources: galaxies

I. INTRODUCTION

During the last three decades, the presence of strong radio emission associated with active galaxies has proved to be one of the most effective ways of pinpointing distant galaxies. Much of the motivation for studying such distant radio galaxies has come from their potential use as cosmological probes (Lilly and Longair 1984; Spinrad and Djorgovski 1987; Rocca-Volmerange 1989) and their ability to provide information about the formation and early history of galaxies.

Most of the previous work on distant radio galaxies has centered on the 3C and "revised" 3CR samples (sources with $S_{178} > 10$ Jy, i.e., the brightest in the northern hemisphere, Bennett 1962; Laing, Riley, and Longair 1983), and the "1 Jy" sample (Allington-Smith 1982; Lilly 1988, 1989*b*). Optical identification of the 3CR sample of radio sources is now nearly complete, and careful spectroscopic investigation of these objects has resulted in the discovery of $\sim$30 radio galaxies with

[1] Visiting Astronomer, National Optical Astronomy Observatories, operated by the Association of Universities for Research in Astronomy, Inc. under contract with the National Science Foundation.
[2] Visiting Astronomer, National Radio Astronomy Observatories, operated by Associated Universities Inc., under contract with the National Science Foundation.
[3] Visiting Astronomer, United Kingdom Infrared Telescope, operated by the Royal Observatory of Edinburgh on behalf of the United Kingdom Science and Engineering Research Council.

redshifts larger than one (Spinrad *et al.* 1985; Spinrad 1987; Djorgovski *et al.* 1988; Spinrad 1989*a*). The most distant 3CR galaxy currently is 3C 257 at $z = 2.474$ (Spinrad 1989*b*) and the most distant "1 Jy" galaxy is 0902+34 at $z = 3.395$ (Lilly 1988).

Recently, with the use of CCDs in the optical, detector arrays in the infrared, and the VLA in the radio, there has been a dramatic increase in our ability to study these distant stellar systems. A crucial development has been the recent discovery of an alignment between the optical/infrared continua and the radio axes in high-redshift radio galaxies (Chambers, Miley, and van Breugel 1987; Chambers, Miley, and Joyce 1988; McCarthy *et al.* 1987*b*). This indicated that their optical and radio properties are in some way related, providing an additional and important incentive for studies of distant radio galaxies.

One approach for extending the search for high-redshift radio galaxies to fainter (and perhaps more distant) sources is to develop techniques for preselecting the best candidates from the large number of radio sources available. We have developed such a method based on the correlation which exists between the radio spectra and luminosities of radio sources (e.g., Heeschen 1960). The most striking manifestation of this correlation was found in the mid-1970s as the byproduct of an investigation of a sample of 4C radio sources having ultrasteep spectra. It was found that the fraction of radio sources which had counterparts on the Palomar Sky Survey was a strong function of the radio spectral index, with almost no identifications for the steepest spectrum sources (Tielens, Miley, and Willis 1978; Blumenthal and Miley 1979). On the reasonable assumption that the unidentified ultrasteep spectrum radio sources were distant galaxies, fainter than the Survey limits, we began a multispectral investigation, with the most sensitive instrumentation now available, of the ultrasteep spectrum radio source sample of Tielens *et al.* This comprised 4C sources known to have spectral indices between 178 and 5000 MHz of $\alpha < -1$, for $S_\nu = k\nu^\alpha$ (Chambers, Miley, and van Breugel 1987; Chambers 1989).

This technique has indeed proved an extremely efficient method to find radio galaxies. We have previously reported on one member of our sample, 4C 40.36, which is a galaxy at $z = 2.267$ (Chambers, Miley, and van Breugel 1988). Here we present the identification and study of the ultrasteep spectrum radio source 4C 41.17 at a redshift of 3.8.

Section II gives an account of the various observations and the relevant data reduction procedures. The observational results are described in § III. Here we give the details of the radiation detected from 4C 41.17 and the physical parameters of the source that can be deduced under standard assumptions (equipartition, photoionization, and recombination, etc.) The section is divided into subsections describing: the determination of the redshift (§ III*a*), the properties of the radio source (§ III*b*), the optical/IR continuum radiation (§ III*c*), and the emission line gas (§ III*d*), and objects detected close to 4C 41.17 (§ III*e*). Section IV contains our discussion of the source within the framework of various scenarios for the physical processes occurring in 4C 41.17 and high-redshift radio galaxies in general. This discussion considers the radio source (§ IV*a*), the optical/IR continuum (§ IV*b*), and the ionized gas (§ IV*e*). We discuss phenomena which may be responsible for shaping the observed morphology and depolarization of the radio source as well as its ultrasteep spectrum. Mechanisms for producing the observed optical/radio alignment effect are considered. Various mixes of stellar populations are shown to be able to produce the observed optical/IR spectral energy distribution (SED). Processes for ionizing and accelerating the Lyα emitting gas are considered. Our conclusions are summarized in § V.

Unless otherwise stated, we shall assume that the universe can be described by a Friedmann cosmology with a Hubble constant of $H_0 = 50$ km s^{-1} Mpc^{-1} and a deceleration parameter of $q_0 = 0.5$.

II. OBSERVATIONS AND DATA REDUCTION

Our investigation of 4C 41.17 comprises radio imaging at three frequencies, optical broad- and narrow-band imaging, optical spectroscopy, and K band infrared imaging. The various telescopes used in this study together with details of the observing configurations, exposure times, dates, and resolutions are given in Table 1. Here "KPNO" refers to telescopes at the Kitt Peak National Observatory, "UKIRT" to the United Kingdom Infrared Telescope on Mauna Kea in Hawaii, and "VLA" to the Very Large Array.

TABLE 1

LOG OF OBSERVATIONS OF 4C 41.17

Date	Telescope	Instrument/ Configuration	Mode	Wavelength/ Frequency	Bandwidth	Exposure	Resolution/ Seeing
1986 May 12	VLA	A array	Continuum	1.465 GHz	50 MHz	15 minutes	1.″2
1986 Aug 4	VLA	B array	Continuum	4.885 GHz	50 MHz	30 minutes	1.2
1986 Dec 15	VLA	C array	Continuum	14.69 GHz	50 MHz	90 minutes	1.2
1987 Jul 15	VLA	A array	Continuum	4.885 GHz	50 MHz	45 minutes	0.4
1988 Dec 15	VLA	A array	Continuum	14.69 GHz	50 MHz	120 minutes	0.11
	VLA	A array	Continuum	1.465 GHz	50 MHz	120 minutes	1.2
1987 Feb 27	KPNO 2.1 m	TI II CCD	Normal	R band	1000 Å	2 × 1800 s	1.2
1988 Jan 21	UKIRT 3.5 m	IRCAM	Raster	K band	2000 Å	40 × 80 s	1.8
1988 Sep 11	KPNO 4 m	PFCCD TI II	Short scan	I band	1000 Å	2 × 3600 s	1.3
1988 Apr 12	KPNO 4 m	PFCCD TI II	Short scan	5830	60 Å	3 × 1800 s	1.8
1988 May 12	KPNO 4 m	PFCCD TI II	Short scan	5830	60 Å	1 × 1800 s	1.0
1988 Mar 10	KPNO 4 m	CRYOCAM	Spectral	500–900 nm	30 Å spatial resolution	1 × 2700 s	1.6
1988 Oct 4	KPNO 4 m	RCSP TI II	Spectral	500–600 nm	2, 4 Å	3 × 900 s	1.6
1989 Feb 8	KPNO 4 m	RCSP TI II	Spectral	300–500 nm	7 Å	3 × 900 s	1.6

a) Radio Imaging

The radio continuum observations of 4C 41.17 were carried out with the VLA as part of our multifrequency study of the 50 radio sources comprising our 4C ultrasteep spectrum sample (Chambers, Miley, and van Breugel 1990). Matched configurations were chosen to give 1".2 resolution at 20, 6, and 2 cm, thereby allowing spectral index distributions to be optimally mapped. Additional A-configuration observations at 6 and 2 cm were carried out in order to delineate fine structure in the radio emission. The fringe amplitudes were calibrated relative to the standard VLA calibrators 3C 48 and 3C 286, and the data were reduced in the normal manner using the NRAO AIPS image processing system. For all the various images, except the 2 cm data (for which the signal-to-noise ratio was insufficient to justify it), the technique of self-calibration was applied to improve the dynamic range of the maps. The final images were constructed after two self-calibration iterations involving phase corrections alone, and one additional iteration involving both phase and amplitude corrections. The error in the absolute radio positions is approximately $\pm 0''.1$.

b) Optical Imaging

The initial CCD image (R band) of the 4C 41.17 field was taken with the 2.2 m telescope at Kitt Peak as part of our program to identify all radio sources in our ultrasteep spectrum sample (Chambers 1989). Using the NRAO measuring machine, astrometric measurements of faint stars on the Palomar Sky Survey which were also present on the CCD image enabled astrometric registration with the VLA radio map and thus the identification of 4C 41.17 (see Fig. 1 [Pl. 1]). The errors in the absolute optical positions, and thus the errors in registration between the optical/infrared images and the radio images, are approximately $\pm 0''.5$. Note the various optical and infrared images are registered by common stars in the field and thus have relative positioning errors of $\pm 0''.1$.

After the redshift had been measured (see below), further imaging was carried out on the 4 m telescope, using the synchronous scanning or "short scan" mode (Schoening 1987) to improve the dynamic range of the image. In this mode, the CCD is moved in the image plane of the telescope by single pixel increments and synchronously read out so that the same part of the image always falls on the same (moving) charge packet. The resultant image is then a composite of many separate short scan frames, each taken with the object slightly displaced to a different part of the chip. This typically improves the flatness of the field and helps eliminate fringing.

The broad-band images were taken with the standard KPNO "nearly Mould" filters and the narrow-band images of redshifted Lyα were taken through an interference filter with a passband of 60 Å centered at 5820 Å. Since the continuum flux of the galaxy is negligible in such a narrow bandpass compared with that of the line, it was not necessary to subtract an off-band image to obtain a map of "pure" Lyα. For all the optical images, data reduction, including flat-fielding and calibration, were carried out using the IRAF imaging analysis software developed by the NOAO. The data were flux-calibrated relative to the standard stars G191 G2B, G140, and the standard field NGC 2264 (Christian *et al.* 1985). The Galactic extinction was derived using $E_{B-V} = 0.15$ (Burstein and Heiles 1982).

c) Infrared Imaging

Infrared observations of 4C 41.17 were made at K band (2.2 μm) on 1988 January 21 using the IRCAM imager on the 3.5 m United Kingdom Infrared telescope. IRCAM utilizes a 58 × 62 InSb focal plane array and camera with a $0''.6$ pixel^{-1} configuration (McLean 1987). Because at 2.2 μm the sky has a brightness of about 13.5 mag arcsec^{-2}, or about 6 mag brighter than those of a typical distant galaxy, it is particularly important to achieve the largest possible dynamic range. To improve the quality of the flat-fielding, we therefore took many images moving the telescope so that our (small) galaxy was observed at several different regions of the chip. An eight-position raster pattern cycle was adopted, reading out the chip every 80 s and spending 4 × 80 s at each position. The total exposure achieved in the observation was 32 × 4 × 80 s = 171 minutes. The infrared images were also reduced using the IRAF software package. After flat-fielding, background subtraction, and flux calibration, it was necessary to shift the individual frames so that they were registered. The scale (pixel separation) was determined from images of fields with stars whose angular separations were measured on the Palomar Sky Survey. The image scale is accurate to $\pm 2\%$. The positioning of the infrared image was determined from star Y, visible in all the final optical and infrared images (Figs. 5 and 6).

The array was flux-calibrated relative to the standard stars HD 162208 and HD 44162, assuming the magnitudes determined by Elias *et al.* (1982) and correcting differentially for atmospheric extinction.

d) Optical Spectroscopy

Our initial spectroscopic observations of 4C 41.17 were made on 1988 March 10 under mediocre seeing conditions, ($\approx 1''.8$) with the Cryogenic Camera (De Veny 1985) at the Cassegrain focus of the KPNO 4 m telescope. By accurately offsetting the telescope from the star denoted by "A" in Figure 1, the $2''.5$ wide, $4'.4$ long slit was centered on the nucleus of 4C 41.17 and oriented at a position angle of 70°, i.e., along the radio source axis. The lowest dispersion grating (810 lines mm^{-1}), and order-sorting red filter GG-420 were used, resulting in a wavelength coverage of 4800–9500 Å with a wavelength resolution of about 30 Å. The pixel separation corresponded to $0''.84$ and about 10 Å in the spatial and wavelength directions, respectively.

These observations were followed up by higher resolution spectroscopy of the detected Lyman-alpha line and a blue spectrum extending the spectral coverage down to the atmospheric cutoff with the Ritchey-Chrétien Spectrograph, the UV Fast Camera, and the TI-II CCD on the 4 m telescope.

The spectroscopic data were also reduced using IRAF. Data reduction consisted of bias-subtraction, flat-fielding, illumination correction, distortion correction, wavelength rectification, sky subtraction, atmospheric extinction correction, and flux calibration relative to the standard star Ross 640.

III. RESULTS

a) The Redshift

Figure 2*a* (Plate 2) shows the low-resolution optical spectrum of 4C 41.17. The one-dimensional extracted spectrum along with the sky spectrum is shown in Figure 3. Two emission lines were detected. The brightest line is centered at 5832 ± 2 Å and a faint one at 7432 ± 2 Å. Although the detection of the faint line is marginal, neighboring features are smaller in width than the instrumental resolution and are in part due to imperfect sky subtraction. The wavelengths of the two lines agree to within the uncertainties with those of Lyα and C IV λ1549 redshifted by $z = 3.800 \pm 0.003$. The fol-

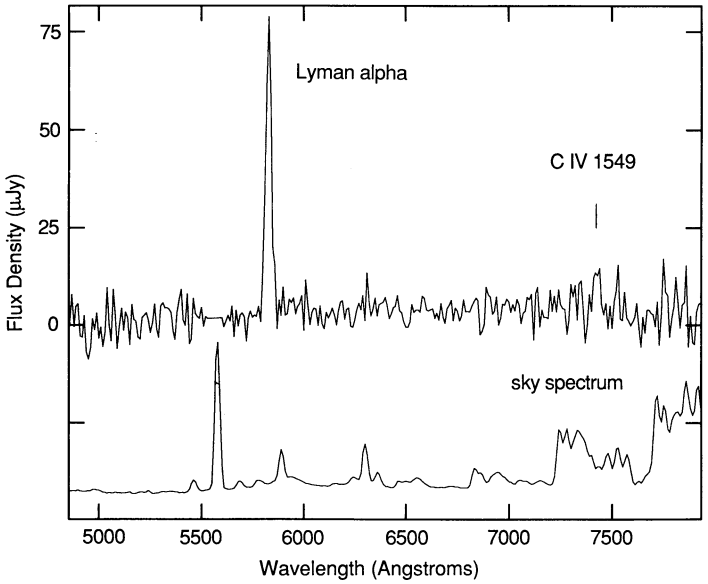

FIG. 3.—Low-dispersion spectrum of 4C 41.17 (*above*) and of the adjacent sky (*below*). Both plots have been derived from the exposure shown in Plate 2, taken with the Cryogenic Camera Slit Spectrograph on the 4 m Mayall telescope with the slit oriented in PA 70°. The plotted spectra have been integrated over the spatial profile (4″) along the slit and smoothed in the dispersion direction over 3 pixels (30 Å) or about one resolution element.

lowing three additional points are supporting evidence that these line identifications are correct:

i) *Line Identifications*

Although our sensitive spectral coverage extends from about 3100 to 8500 Å, no other lines from the galaxy were detected. If the strong line at 5832 Å was [O II] λ3727 at a redshift of 0.565, then not only is the line at 7432 Å inexplicable, but our upper limits on the ratios of [O II] λ5007 to [O III] λ3727 is 0.1 and of Mg II λ2799 to [O II] λ3727 is 0.1. These flux ratios would be unusually small for conventional radio galaxies (Spinrad 1986). Our spectrum shows no evidence of He II λ1640, but given the chip sensitivity and sky noise, this nondetection does not indicate an anomalous He II/C IV ratio (Spinrad 1986).

ii) *Continuum Feature*

The continuum drops by more than a factor of 3 shortward of the strongest line (§ IIIc). This sharp falloff is observed in both the low- and high-resolution spectra. This feature is consistent with either a depression of the continuum by the Lyα forest or a drop in the stellar continuum shortward of Lyα.

iii) *K Magnitude*

The measured K band flux density of 4C 41.17 (see below) is consistent with the K magnitude–redshift diagram (Lilly and Longair 1984) for a redshift of 3.8. If the bright line at 5836 Å were λ3727, at a redshift of 0.6, the K band flux would be underluminous by almost 3 mag and thereby considerably discrepant in the K magnitude–redshift diagram. However, this is a statistical argument since some underluminous radio galaxies exist (Chambers, Miley, and van Breugel 1990).

iv) *Radio Spectrum*

From Figure 9 we note that at an observed frequency of 26 MHz there is still no hint of any low-frequency turnover due to synchrotron self-absorption. This phenomena typically occurs around 75–100 MHz. Therefore the lack of such a feature is further circumstantial evidence that we are observing a much higher rest frame frequency.

We shall therefore henceforth in this paper take the redshift of 4C 41.17 as being 3.800 ± 0.003. At this redshift, conversion to intrinsic parameters depends severely on the assumed cosmology. For example, $1'' = 6.6$ kpc at $z = 3.8$ for $H_0 = 50$ km s^{-1} Mpc^{-1} and $q_0 = 0.5$, but this could be a factor of 2 smaller or larger depending on the value of H_0 or q_0, leading to an uncertainty in the derived volume of an order of magnitude.

b) *The Radio Source*

Figure 4 is a montage of several of the resultant radio images at different scales and resolutions. Some relevant parameters directly measured from these data are tabulated in Table 2. The following should be noted from the radio observations:

i) *Classification*

The overall morphology is that of a classical double or "FR Type II," with edge brightened outer lobes. The structure and enormous 178 MHz luminosity of 4C 41.17 (Table 2) are consistent with the relation between morphology and luminosity of radio sources at lower redshifts first demonstrated by Fanaroff and Riley (1974). However, in contrast to the case for many edge-brightened sources, more than half the flux is radiated by the central components (B_1, B_2, and B_3).

ii) *Structure and Orientation*

The large-scale structure of 4C 41.17 can be considered as three components, "A," "B," and "C" separated by $\sim 6''$ and not quite collinear with an average position angle of $48° \pm 5°$. Component B is most closely associated with the optical peak. The inner component B is itself composed of three subcomponents (B_1, B_2, and B_3) and has a size of $\sim 4''$ and position angle of 74°. This component is extremely well aligned with the inner Lyα emission to within 3°.

iii) *Core*

No flat spectrum core, the usual designator of the radio "nucleus," was detected. The maximum of the infrared continuum image is consistent with either B_1 or B_2 or somewhere in between. Many radio galaxies have no detectable radio core, and this may be the case with 4C 41.17. We note that the extremities of A and C are collinear to $\pm 9°$ with the most compact component B_1, consistent with B_1 being the center or near the center of radio activity.

iv) *Northeastern Component C*

This very faint extended feature is extended along a position angle of $\sim 74°$, i.e., in a similar direction to the inner component, B, and different from the overall source orientation.

v) *Spectral Index Distributions*

Although all components have ultrasteep radio spectra (see Table 2 and Fig. 4), there are spectral index variations between them, B being the flattest (~ -1.3) and the northeast component C having an extremely steep spectral index ($\lesssim -3$).

vi) *Polarization Distributions*

From Table 2 it can be seen that no polarization was detected except for B_3 at 4.8 GHz which has a 14% polarization at a position angle of 32°. The 3 σ upper limits for B_1 and A are 20% and 8%, respectively, at 4.8 GHz and 30%, 2%, and 1% for components C, B_1, and A, respectively at 1.4 GHz. This implies that B_1 and A are already severely depolarized at very short wavelengths (3.0 and 1.3 cm in the emitted frame).

TABLE 2

OBSERVATIONAL PARAMETERS OF THE RADIO EMISSION OF 4C 41.17

COMPONENT (1)	R.A. (1950) (2)	DECL. (1950) (3)	ANGULAR SIZE (4)	POSITION ANGLE (5)	FLUX DENSITY 1.465 GHz (mJy) (6)	FLUX DENSITY 4.885 GHz (mJy) (7)	FLUX DENSITY 14.69 GHz (mJy) (8)	SPECTRAL INDEX α_{1465}^{178} (9)	SPECTRAL INDEX α_{4885}^{1465} (10)	SPECTRAL INDEX α_{14695}^{4885} (11)	PERCENT POLARIZATION (P) (6 cm) (12)	BEAM (13)
Integrated:	...	...	...	...	210(10)	39.8(2.0)	6.4(0.6)	−1.23	−1.38(0.09)	−1.65(0.15)	...	1.″2
A	06^{h}47^{m}20.^{s}012	41°33′59.″3	4.″2 × 3.″8	52°	75(4)	10.7(0.5)	0.3(0.2)	...	−1.62(0.09)	−3.25(1.0)	...	1.2
B	...	...	4.8 × 3.2	74	126(6)	28.7(1.5)	6.0(0.6)	...	−1.23(0.09)	−1.42(0.14)	...	1.2
B_1	06 47 20.527	41 34 03.6	2.0 × 2.0	74	29.3(1.5)	5.0(0.3)	<0.9	...	−1.47(0.09)	< −1.66	...	1.2
$B_{2,3}$	...	...	2.5 × 2.5	74	95(5)	23.2(1.0)	5.2(0.5)	...	−1.17(0.09)	−1.35(0.16)	14	1.2
C	06 47 20.880	41 34 07.7	5.0 × 3.0	43	10.4(0.5)	<0.3	<0.9	...	< −2.94	...	...	1.2
A	...	...	0.9 × 0.9	...	...	9.5(0.5)	...	...	...	...	...	0.4
B	...	...	3.5 × 1.8	...	...	27.1(1.5)	...	...	...	...	...	0.4
B_1	...	...	0.4 × 0.4	...	...	4.1(0.3)	...	...	...	...	...	0.4
$B_{2,3}$	...	...	1.3 × 1.3	...	...	22.8(1.0)	...	...	...	...	...	0.4
B_1	...	...	0.11 × 0.11	...	...	...	0.9(0.2)	...	...	...	...	0.11
B_2	06 47 20.628	41 34 04.1	0.11 × 0.11	...	...	...	1.4(0.2)	...	...	...	...	0.11
B_3	06 47 20.676	41 34 04.3	0.11 × 0.11	...	...	...	2.3(0.3)	...	...	...	...	0.11

NOTE.—Errors in absolute flux are given in parentheses next to the value and are derived from the 1 σ absolute calibration error and rms image noise added in quadrature. Upper limits are for 3 σ detections. Approximate spectral index errors are given in parentheses next to the value and are derived from the 1 σ flux errors.

TABLE 3

PHYSICAL PARAMETERS OF THE RADIO EMISSION OF 4C 41.17

COMPONENT (1)	4.8 GHz MONOCHROMATIC LUMINOSITY (10^{27} W Hz^{-1}) (2)	TOTAL RADIO LUMINOSITY (10^{45} ergs s^{-1}) (3)	LARGEST LINEAR SIZE (kpc) (4)	MAGNETIC FIELD STRENGTH (10^{-4} G) (5)	MINIMUM THERMAL PRESSURE (10^{-9} dyn cm^{-2}) (6)	MINIMUM TOTAL ENERGY (10^{60} ergs s^{-1}) (7)	RADIATIVE LIFETIME AT 6 cm (10^4 yr) (8)	$(n_e)_{ext}$ Ram $v = 10^3$ km s^{-1} cm^{-3} (9)	$(n_e)_{ext}$ Thermal $T = 10^{-8}$ cm^{-3} (10)
Integrated	8.5	11	~100	...	...	...	...	...	...
A	2.2	3	32	1.5	1.3	0.8	4	0.07	0.03
B	4.8	4	32	1.5	1.3	0.9	7	0.07	0.03
B_1	1.2	2	13	2	3	0.4	4	0.2	0.07
$B_{2,3}$	3.5	2	16	2	2	0.4	6	0.2	0.04
B_2 fraction unresolved	0.9	0.6	0.7	17	200	0.003	0.2	10	4
B_3 fraction unresolved	1.6	1.0	0.7	20	200	0.004	0.2	13	5
$H_0 = 50$, $q_0 = 0.01$	4.2	4.2	2.1	0.82	0.66	5.7	1.3	0.66	0.66
$H_0 = 100$, $q_0 = 0.01$	1.05	1.05	1.02	0.99	0.99	1.06	1.01	0.99	0.99

NOTE.—Values derived from minimum energy arguments using standard assumptions quoted in the text. Values for *A* were derived using the integrated spectral index, since the high-frequency spectral index would overestimate the luminosity of *A*.

vii) *Derived Physical Parameters*

Table 3 gives some intrinsic parameters in the emitted frame for the 4C 41.17 radio source and its various components derived using the data in Table 2 combined with the assumptions usually adopted in interpreting radio sources (e.g., Miley 1980; Pacholczyk 1970). In calculating the minimum energies, we assumed that the radio source is cylindrically symmetric, has unit filling factor, and that the emitted synchrotron spectrum extends from 10^7 to 10^{11} Hz. Furthermore, assuming primordial abundances $X = 0.76$, $Y = 0.24$, we calculate the electron density $n_e = \rho/2m_p\ (1 + X)$ of an external medium needed to confine the equipartition pressure of the radio source on the basis of (1) ram confinement by a gas with a relative velocity of $v = 1000$ km s^{-1}, ($P_{eq} = \rho v^2$) and (2) thermal confinement by a gas at $T = 10^8$ K ($P_{eq} = 2n_e kT$). The average radiative lifetimes were calculated at 4.885 GHz, where the spectrum steepens.

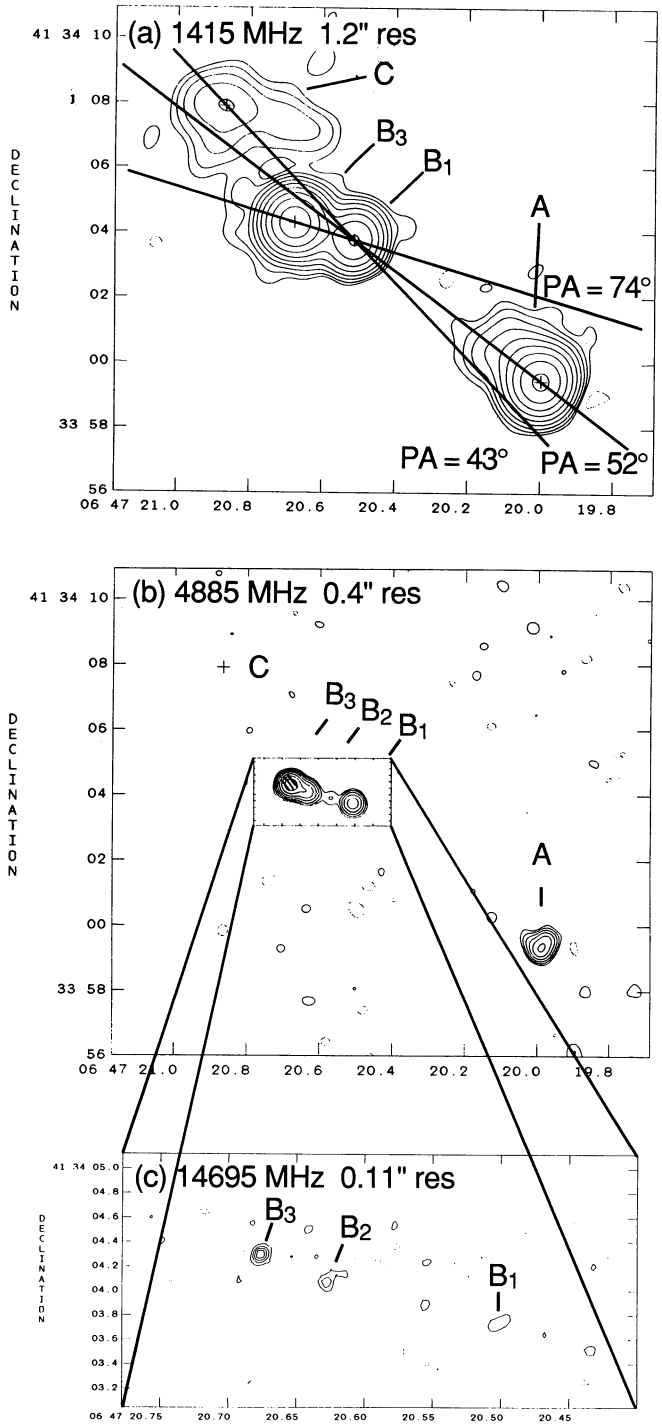

FIG. 4.—The radio structure of 4C 41.17 as imaged with the VLA in the A array. (*a*) Map made at 1465 MHz (20 cm) (1.″2 FWHM resolution). Contour levels are −0.2, 0.2, 0.4, 0.8, 1.6, 3.2, 6.4, 12.8, 25.6, and 51.2 mJy per beam. (*b*) Map made at 4885 MHz (6 cm) (0.″4 FWHM resolution). Contour levels are −0.15, 0.15, 0.3, 0.6, 1.2, 2.4, 4.8, 9.6, 19.2, 38.4, and 76.8 mJy per beam. (*c*) Map made at 14695 MHz (0.″11 FWHM resolution). Contour levels are −0.4, 0.4, 0.8, 1.2, and 1.6 mJy per beam.

At the redshift of 3.8, the cosmology adopted has a significant effect on many of the physical parameters, so although the parameters have been calculated for $q_0 = 0.5$, below each column we give a multiplicative factor for which the change to the parameters for a $q_0 = 0.01$ can be calculated.

c) The Optical/Infrared Continuum

Montages of the radio, optical, and infrared morphologies are presented in Figures 5 and 6 (Plate 3). Contour maps of the *R* band, *I* band, and 2.2 μm *K* band images are shown in Figures 5*d*, 5*e*, and 5*f*. Note that the *K* band 2.2 μm image is roughly equivalent to a *V* band image in the rest frame. Bright stars are present in both the optical and infrared images, allowing the spatial registration of the frames to an accuracy of better than 0.″1. Integrated apparent and absolute magnitudes for 4C 41.17 are listed in Tables 4 and 6, respectively.

Care must be taken in interpreting these data to allow for possible "contamination" of the broad-band images by emission lines. The *R* band data is definitely contaminated by Lyman-alpha at 5830 Å. In addition, the *K* band data may be slightly affected by the [O III] λ5007 emission line at 2.403 μm; however, this is at the edge of the bandpass where the filter transparency is reduced over the peak by at least a factor of 2. Taking typical ratios of Lyα to [O II] λ3727 of 6 (Spinrad 1986) and a ratio of [O III] λ5007 to [O II] λ3727 of 3 for Cygnus A (Osterbrock 1989), the [O III] λ5007 could be as large as half the Lyα flux. However, the observed equivalent width would have to be greater than 1200 Å to account for half the *K* band flux if the line were centered in the band. This argument implies that [O III] λ5007 must contribute less than 25% of the measured flux at *K* band and probably contributes less than 12%. Although the C IV λ1550 emission line falls into the *I* band filter our spectroscopy indicates that it contributes less than 5% of the flux in the band, so the *I* band image of Figure 5*e* and Figure 6*e* can safely be taken as representative of the ultraviolet (rest frame) continuum emission.

To obtain further data on the behavior of the SED, we also applied an aperture correction to a heavily smoothed (with emission lines excised) version of our fluxed Cryocam spectra. The continuum was then averaged over 100 Å bins, and these data points are plotted as small boxes in Figure 7.

We note the following properties of the continuum emission:

i) *Structure and Orientation*

There is emission on several distinct spatial scales—an inner unresolved component; a component having a size of about 4″, aligned roughly along the radio source, corresponding with the "galaxy" component of the gas; and a halo component which extends by at least 15″. We shall designate these "peak," "galaxy," and "halo," respectively. The halo component of the

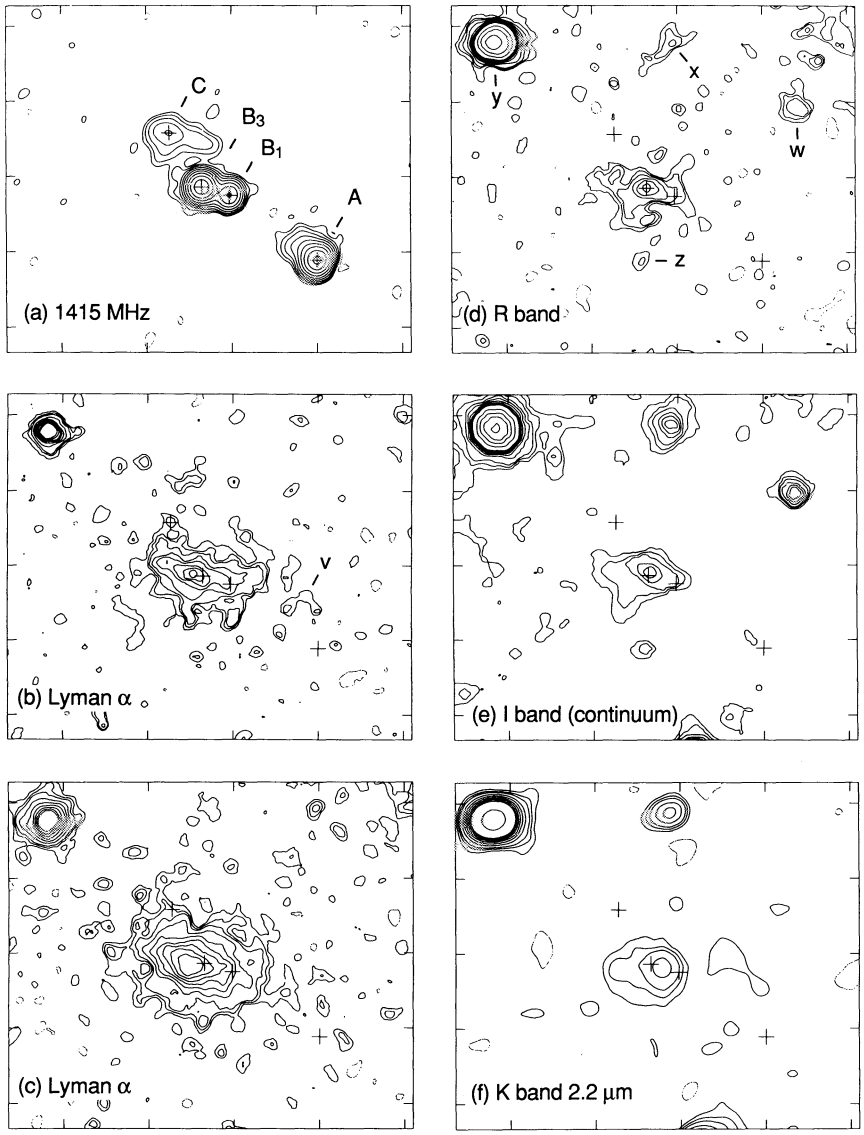

FIG. 5.—Radio, infrared, and optical images of 4C 41.17. (*a*) VLA 4885 MHz. Same as Fig. 2*a*. (*b*) Best seeing Lyα image. (~1.″0 FWHM resolution). Contour levels are ~ −2, 2, 3, 4, 5, 6, 7, and 8 σ. (*c*) Smoothed Lyα image (~2″ FWHM resolution). Contour levels are ~ −2, 2, 3, 4, 5, 6, 7, 8, 9, and 10 σ. (*d*) *R* band (~1.″2 FWHM resolution). Contour levels are ~ −2, 2, 3, 4, 5, 6, 7, 8, 9, and 10 σ. (*e*) *I* band (~1.″3 FWHM resolution). Contour levels are ~ −2, 2, 3, 4, 5, 6, 7, 8, 9, and 10 σ. (*f*) Smoothed *K* band image (~2″ FWHM resolution). Contour levels are ~ −2, 2, 3, 4, 5, 6, 7, 8, 9, and 10 σ.

Crosses indicate the positions of the peak intensities of the radio components from Fig. 3*a*. Tick marks are given at intervals of 5″. The relative registration of the optical/infrared images was carried out using stars on the images and is accurate to ~0.″1; the radio/optical registration is accurate to ~0.″5.

continuum has an extension to the southeast which is neither present on the radio map nor on the image of the Lyα.

ii) *Spectral Energy Distribution*

The spectral energy distribution of 4C 41.17 indicated by the optical/infrared measurements (Fig. 7) is not as red as the "1 Jy" source 0902+34 at $z = 3.395$ as published by Lilly (1988). However, the *K* band flux of 0902+34 may be somewhat smaller than originally reported (Lilly 1989*a*) which would then make the SED of 0902+34 similar to that of 4C 41.17.

The main features of the SED are as follows:

1. A sharp falloff shortward of Lyα. The two 100 Å wide data points shortward of Lyα (centered at 990 Å and 1090 Å) indicate nearly an order of magnitude decrease in the continuum from that at 1340 Å. This decrease can also be seen in Figure 2*a*. However the shortest wavelength point in Figure 7 is affected by the decrease in the chip sensitivity below 5000 Å, hence the increased uncertainty.

2. A "1500 Å break" similar to that found in the summed spectra of high-redshift radio galaxies by Chambers and McCarthy (1990). Although the signal-to-noise ratio is poor, the feature persists with a wide variety of smoothing scales.

3. A relatively "flat" component in the rest frame ultraviolet from ~1500 to ~2000 Å.

4. A "red bump" defined by the *K* band measurement at about 4600 Å in the rest frame, similar to that observed in 0902+34 (Lilly 1988). The continuum flux must increase sharply with wavelength somewhere between about 2500 and 4600 Å to produce this red bump.

TABLE 4

OBSERVATIONAL PARAMETERS OF THE OPTICAL/INFRARED EMISSION OF 4C 41.17

Component (1)	R.A. (1950) (2)	Decl. (1950) (3)	Projected Area (4)	Lyα Flux (10^{-15} ergs s^{-1} cm^{-2}) (5)	Observed Lyα Equivalent Width (Å) (6)	Lyα FWHM (km s^{-1}) (7)	Lyα FWZM (km s^{-1}) (8)	C IV 1549 Flux (10^{-15} ergs s^{-1} cm^{-2}) (9)	R_{mag} (10)	I_{mag} (11)	K_{mag} (12)
Peak	$06^h47^m20^s.793$	41°34′04″.5	1″.2 × 1″.2	2.2(1)	1300(200)	900	...	0.2	23.8(1.0)	23.3(1.0)	20.8(1.0)
Galaxy	...	...	6 × 4	3.5(2)	1000(200)	1000	...	...	22.0(0.5)	22.0(0.5)	18.7(0.5)
Halo + Galaxy	...	...	15 × 10	5(2)	>500	800	...	...	21.7(0.5)	21.8(0.5)	18.6(0.5)
"Jet"			1.2 × 6	>0.1	...	...	2500	...	...	...	...
"Disk"			~15	>0.1	...	100	...	...	...	...	...
"z"	06 47 20.695	41 33 59.5	...	...	...	...	...	...	...	...	...
"v"	06 47 20.185	41 34 02.2	...	...	...	...	...	...	...	...	...
Galaxy w	06 47 19.821	41 34 09.8	...	...	...	...	...	...	...	...	...
Galaxy x	06 47 20.540	41 34 14.4	...	...	...	...	...	...	...	...	...
Star y	06 47 21.570	41 34 14.1	...	...	...	...	...	...	...	...	...
Star A	06 47 19.136	41 34 24.2	...	...	...	...	...	...	...	...	...

NOTE.—Errors (1 σ) are given in parentheses next to the values. The velocities are in the rest frame. The photometry is for the total rectangular aperture quoted.

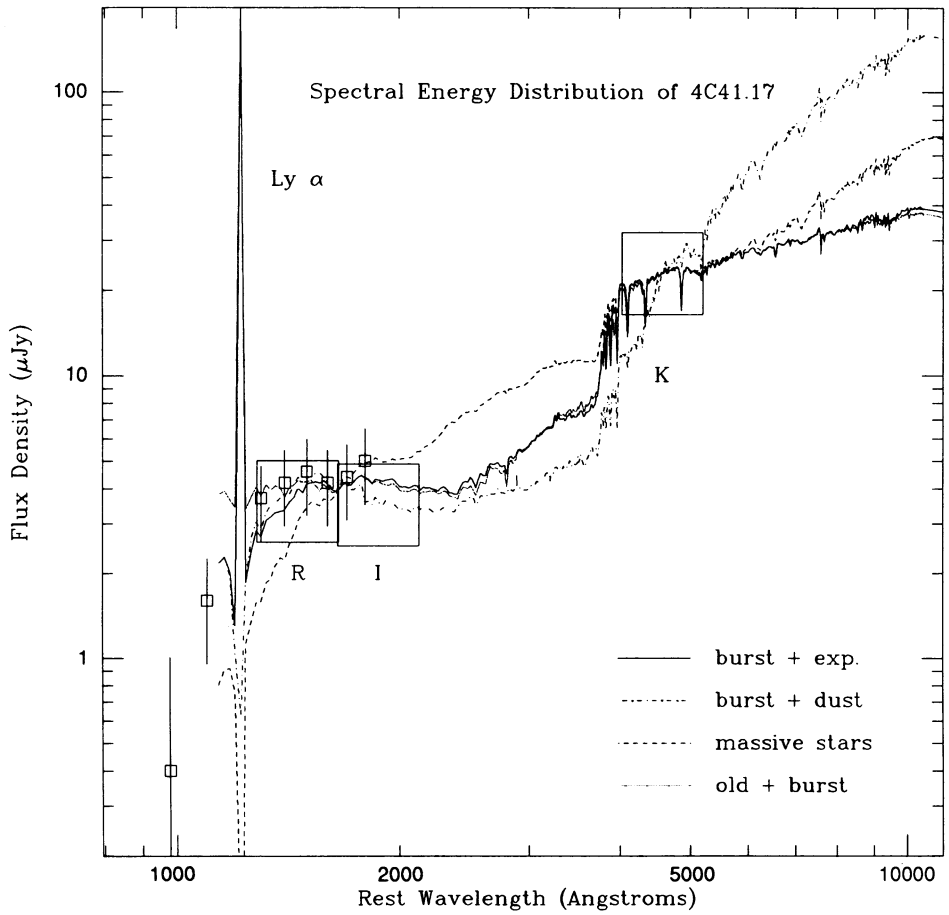

FIG. 7.—Spectral energy distribution ("SED") of 4C 41.17. Integrated optical and infrared measurements from *R*, *I*, and *K* band images (*large boxes*) and low-dispersion spectrum (*small boxes*). The four models shown are discussed in the text.

iii) *Color Gradients*

Comparison of the profiles taken through the images at the different wavelengths show that the peak intensities gradually shift in position as a function of wavelength. In particular, the *K* band peak is to the west of the (gas-uncontaminated) *I* band peak, whereas the Lyα peak is located tc the east of the *I* band peak. This implies a color gradient that is systematically bluer eastward along the radio axis (see Fig. 8). These gradients are a small percentage of the integrated light and thus will change the SED for each region only slightly.

d) Line Emission

A description of the gas in 4C 41.17 is given by the narrow-band images at two different spatial resolutions (Figs. 5*b*, 5*c*, 6*b*, and 6*c*), as well as the slit spectra (Figs. 2 and 8*a*). Figure 8*a* shows a contour of velocity of the Lyα gas plotted against distance along the slit spectrograph, aligned in position angle 70° along the radio source axis. Observational parameters of the gas derived from the narrow-band images are tabulated in Table 4. Several points are apparent:

i) *Structure and Orientation*

The gas extends over a region of more than 10″ × 15″ corresponding to a linear size of ~100 kpc. The images are consistent with the slit spectra taken along the radio position angle which also indicates that the gas has an extent of at least 15″. There appear to be three spatially distinct scales in the gas: (1) the "jet component" with a size of 4″ × 2″ (26 × 13 kpc); (2) the "galaxy component," with a size of about 8″ × 3″ (52 × 20 kpc), closely coincident with the inner *B* radio component; and (3) a "halo component" ≳18″ × ≳10″ (120 × 66 kpc). (Note that in the narrow-band image the extent of the halo is evident only out to ~15″, however from the deeper high-resolution spectroscopy, i.e., Figs. 2 and 8*a*, it is clear that the halo extends at least 18″ in one direction.) All three components of the gas have similar orientation with a PA of 74°, i.e., coincident with the axis of the central radio component, *B*. Although the halo is considerably larger than the overall radio source, it appears to share this same axis.

ii) *Wiggle Feature*

The morphology of the gas (Fig. 5*b* and 6*b*) exhibits a "wiggle" with a scale length of about 3″ (20 kpc) and an orientation change of about 45°. Note that the scale length is comparable with the radio component separation and the orientation change is similar to that of the position angle difference between the inner and outer radio structure.

iii) *Velocity Field*

The velocity field of the emission-line gas is complex and in particular shows no clear evidence of large scale rotation (see Figs. 2*c*, 2*d*, and 8*a*). There are at least four components: a high-velocity component associated with the radio jet, a clumpy turbulent field associated with the continuum emis-

sion, the extended halo, and a cold component about 500 km s^{-1} blueward of the peak. The high-velocity component of the gas encompasses a range of more than 2000 km s^{-1} over an angular scale of about 5″, which is well correlated spatially with the inner radio component *B*. In addition, there are numerous clumps and features (Fig. 2*c*) whose existence require confirmation.

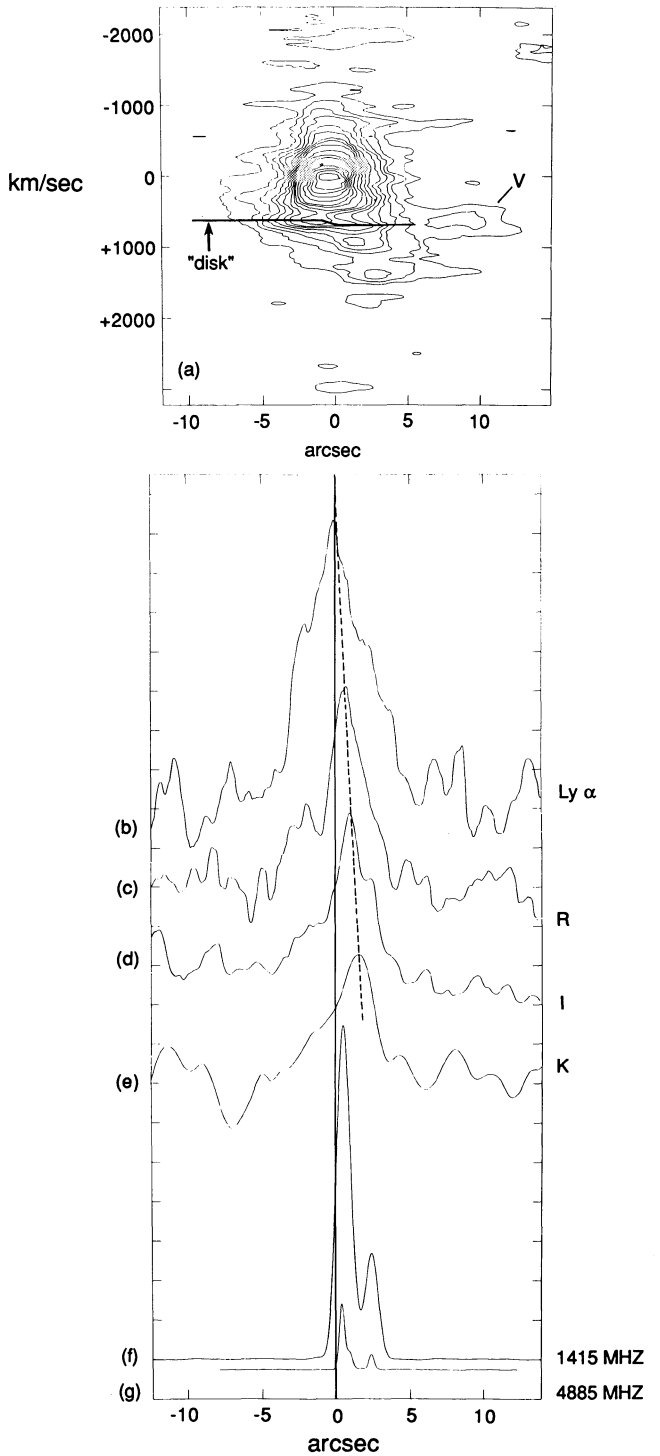

FIG. 8.—Velocity contours (*above*) and intensity profiles (*below*) obtained approximately along the radio axis (PA 70°). East is to the left. The intensity profiles are relative, determined by averaging 2″ wide slices from broad-band images. Ticks and positional alignment are as for Fig. 3.

The large-scale motion of the gas is complex and cannot be described by simple organized motion such as pure rotation. The velocity dispersion of the inner "galaxy" region ($\sim$400 km s^{-1}) is somewhat larger than that of the "halo" component ($\sim$300 km s^{-1}), but these are difficult to distinguish, and the bulk of the gas shows no organized motion. In addition, there is one feature (better visible in Fig. 2*d* than Fig. 8*a*) that shows a cold component with a velocity gradient of $\sim$100 km s^{-1}. We refer to this component as the "disk" and note that is 500 km s^{-1} blueward of the peak. It is also well matched in velocity to the component "v" which is marked on the narrow-band image (Fig. 5*b*) and in Figure 8*a*.

iv) *Clumpiness*

Both the images and the spectra suggest that the gas is clumpy down to the limit of our spatial resolution ($\sim$1″) and the limit of our velocity resolution of $\sim$100 km s^{-1}.

v) *Derived Physical Parameters*

Unfortunately there are few diagnostics which enable the density and state of the ionized gas to be deduced. Furthermore, as discussed in § IV*c*, there may be significant contributions of ionizing photons from different sources, e.g., stellar photospheres, the nucleus, and the radio source. Nonetheless an estimate of the density and a corresponding estimate of the mass of the gas can be obtained by assuming a filling factor f and calculating the electron density n_e necessary to produce the observed Lyα luminosity from the observed volume: $n_e = 0.058 L_{44} f^{-1/2} V_{70}^{-1/2}$ cm^{-3}, where L_{44} is the Lyα luminosity in 10^{44} ergs s^{-1}, V_{70} is the volume in 10^{70} cm^3, and assuming a recombination coefficient $\alpha_{rec} = 2.87^{-24}$ ergs cm^3 s^{-1} for partially ionized low-density regions (Osterbrock 1989). Volume-filling factors have been determined for local radio galaxies from direct measurements of the densities and values have a large dispersion, covering a range from $\sim 10^{-4}$ to $\sim 10^{-6}$ (e.g., van Breugel 1985; Heckman *et al.* 1982). We will adopt a value of $f = 10^{-5}$ in model 2, below.

An alternative method of estimating the density is to assume a model where the Lyα luminosity is due to photoionization from an obscured central nucleus, and estimate the ionizing flux and an ionization parameter. Note that while such a model is reasonable for some objects (Baum and Heckman 1989*a*; McCarthy *et al.* 1990), it is less than satisfactory for 4C 41.17 since greatly extended ultraviolet continuum is observed and much of the photoionization may be local, i.e., due to stars. This is a crucial point, since these distributed sources of ionizing photons will make an important contribution to the state of the gas regardless of the nucleus. For purposes of discussion, however, we can assume a "unified" picture and use values for the ionization parameter consistent with other active nuclei. For a nonthermal ionizing continuum of spectral index $\alpha = -1.5$, typical values of the dimensionless ionization parameter are $\log(U) \sim -3.5$, -2.5, and -2.0 for LINERs, Seyferts, and quasars respectively (e.g., Ferland and Netzer 1983; Halpern and Steiner 1983). Spatially unresolved C IV 1549 is observed in 4C 41.17, and therefore it seems likely there is some nuclear nonthermal continuum. For the "unified models" below, we will adopt a value of $\log(U) = -2.5$ which gives reasonable agreement with the line ratios of lower redshift radio galaxies (McCarthy 1989).

The greatest uncertainty in the case of 4C 41.17 is the magnitude of the ionizing flux, since the nucleus is obscured in our

TABLE 5

PHYSICAL PARAMETERS OF THE LYMAN-ALPHA EMISSION-LINE GAS OF 4C 41.17

Component (1)	Lyα Luminosity (10^{44} ergs s^{-1}) (2)	Estimated Volume (10^{70} cm^3) (3)	Model (4)	n_e cold ($\sim 10^4$ K cm^{-3}) (5)	log Filling Factor (6)	log Cover Factor (7)	log U at R_{23} (8)	Mass Emission-Line Gas (10^7 $M_\odot$) (9)	Velocity Dispersion (km s^{-1}) (10)	Kinetic Energy (10^{56} ergs) (11)	Pressure (10^{-9} dyn cm^{-2}) (12)	n_e hot ($\sim 10^7$ K cm^{-3}) (13)
Peak	2.6	0.001	1	400	−4.4	0	−2.5	6400	400	1000	0.004	0.0006
			2	900	−5	−2	−3.3	10	400	1.4	2	0.4
			3	1400	−5.4	−3	−2.5	6	400	1.0	4	0.6
Galaxy	4.1	0.6	1	700	−6.3	0	−2.5	6400	400	1000	0.006	0.0010
			2	150	−5	−2	−3.3	100	400	17	0.4	0.07
			3	2000	−7.4	−3	−2.5	6	400	1.0	6	1
Integrated	5.8	1.6	1	900	−7.9	0	−2.5	6400	350	700	0.009	0.0014
			2	30	−5	−2	−1.3	600	350	70	0.1	0.016
			3	3000	−8.9	−3	−2.5	6	350	0.7	9	1.4
Halo = Integrated − Galaxy	1.7	1.6	1	300	−7.4	0	−2.5	6400	350	700	0.003	0.0004
			2	20	−5	−2	−1.8	300	350	40	0.05	0.01
			3	900	−8.4	−3	−2.5	6	350	0.7	3	0.4
$H_0 = 50$, $q_0 = 0.01$	4.2	8.6	...	0.7	1.0	1.0	6.0	6.0	1	6.0	0.7	0.7
$H_0 = 100$, $q_0 = 0.01$	1.05	1.07	...	0.99	1.0	1.0	1.06	1.06	1	1.06	0.99	0.99

NOTE.—Physical parameters derived from observed Lyman-alpha flux and apparent size. Values are given for a range of assumptions indicated by models (1), (2), and (3) as discussed in the text.

direction and we have no direct measurement of it. As we will see in the calculations presented below and in Table 5, in a model where the ionizing continuum is dominated by the nucleus, then in order to obtain both pressures consistent with the interpretation of the radio source data and ionization parameters comparable to known AGNs, the Lyα-emitting clouds must intercept only a small fraction of the ionizing continuum from the nucleus, i.e., it is necessary to introduce a covering factor f_c of order $0.01 \sim 0.001$.

For convenience we will assume that the density of the clouds decreases as r^{-2} in which case the ionization parameter and hence the degree of ionization at the front surface of all clouds is independent of distance. Then for a characteristic size $R_{23} = R/10^{23}$ cm, characteristic n_e, and assuming each Lyα photon represents one ionizing photon from the nucleus, the ionization parameter is $U = 1.63 \times 10^{-3} f_c L_{44} R_{23}^{-2} n_e^{-1}$.

In Table 5 we estimate the physical parameters in each physical region of 4C 41.17 from the observed Lyα flux and size of the emitting region for each of three sample "models:" (1) filling factor determined by covering factor $f_c = 1$ and ionization parameter $\log(U) = -2.5$, (2) ionization parameter determined by a filling factor 10^{-5} and covering factor $f_c = 0.01$, and (3) filling factor determined by covering factor $f_c = 0.001$ and ionization parameter $\log(U) = -2.5$. Model (2) assumes a uniform mass distribution, whereas in models (1) and (3) the mass in the emission line clouds is distributed as r^{-2}.

With values of the electron density estimated in this crude fashion we go on to estimate the mass of the emission line gas $M = \mu m_p V f$, the kinetic energy $\mathrm{KE} = 0.5 M\sigma^2$, the pressure $P = 2 n_e kT$ where we assume $T = 10^4$ K, and the electron density in a hot (10^7) phase in pressure equilibrium with the emission-line gas for each "model." We have assumed the above primordial abundances and therefore a mean molecular weight $\mu = 1.22$ for the neutral gas. Just as for Table 3 we also show the multiplicative factors applicable to each column in the cases, where q_0 is 0 and 0.5 and H_0 is 100 km s^{-1} Mpc^{-1}.

Note that while none of the crucial parameters can be independently determined to within an order of magnitude, the application of a self-consistent model does constrain somewhat the plausible region of parameter space. The gas pressure suggested by the radio cocoon model discussed in § IV*b*(iii) favors model (3), where the emission line gas has $n_e \sim 1000$ and $M \sim 6 \times 10^7 M_\odot$.

e) Possible Companions to 4C 41.17

i) *Component Z*

The object marked "z" in the *R* band image of Figure 5*d*, 5″ south of 4C 41.17 is marginally detected in the other images, including Lyα although the *K* band detection is not very convincing. However, these are all completely independent measurements. Note that given its continuum flux, it should not have been detected in the narrow-band image unless there is line emission at the same wavelength as Lyα in 4C 41.17. Therefore, this object may be a companion or a component of the 4C 41.17 system.

ii) *Field Objects*

We identify the objects marked "x" and "w" in Figure 5*d* as possible galaxies, since they appear to be extended. They are not detected in the narrow band image of 4C 41.17, so presumably they do not have strong emission lines in that waveband. Therefore they are probably foreground galaxies. We note that object "x" is significantly redder than 4C 41.17, while object "w" is bluer. Deeper observations of the 4C 41.17 field are desirable to investigate whether any of the field objects could be at the distance of 4C 41.17.

IV. DISCUSSION

a) The Radio Source

i) *Morphology*

From the morphology of the radio source we infer various processes which may be occurring:

1. Precession

As we pointed out in § III, the radio source is not collinear; there appear to be two distinct axes in the system, the inner axis defined by component *B* is $\sim 20°$ different from the outer orientation defined by components *A*, B_1, and *C*. The resemblance of the radio morphologies of components *C* and *B* at first sight suggests that *C* could be a gravitationally lensed image of *B*. However, this explanation can be ruled out since the radio spectral indices of these components are significantly different and gravitational lenses should be achromatic. A more likely explanation of the symmetry is that it is due to a time-dependant wobbling or precession in the nuclear "ejection" axis.

2. Interaction with the Ambient Medium

From observations of radio galaxies at lower redshift such as 3C 277.3 (van Breugel *et al.* 1985), which have extended line emission morphologically related to the radio source, it has been shown that interaction with the line-emitting gas can bend, decollimate, and depolarize the radio source as well as possibly produce "knots" of enhanced radio emission (e.g., Miley 1981; van Breugel 1986). The similarity of the radio and Lyman-alpha structures implies that 4C 41.17 must also be influenced considerably by such interactions. A gas cloud such as that designated by "v" in Figure 8*a* at 500 km s^{-1} relative to the peak of the Lyα, may have been responsible for bending the radio jet.

3. Depolarization

The low radio polarizations at the relatively short rest wavelengths are almost certainly related to the presence of the ionized gas indicated by the Lyα emission. For the range of gas densities in Table 5, together with equipartition magnetic field strengths and path lengths from Table 3, the resultant Faraday rotations are typically a few hundred radians at the rest wavelength of 1.25 cm, corresponding to our most stringent 6 cm polarization limits (Table 2). It is therefore highly probable that such a medium would result in strong depolarization of the radio source.

ii) *Ultrasteep Spectrum*

Why is the radio spectrum so steep? All the radio components *A*, *B*(i), (ii), (iii) have spectral indices $\alpha < -1.2$ between observing frequencies of 1.4 and 5 GHz. Less than 5% of sources detected in low-frequency surveys such as the 4C have as steep spectra. However, as we discussed above, the ultrasteep spectrum sources tend to be the most powerful and distant ones. The statistics are not yet sufficient to distinguish whether the ultrasteep spectra are more related to the luminosity of a source or its distance (e.g., Blumenthal and Miley 1979).

Several processes could contribute to producing the observed steep radio synchrotron spectrum and be responsible

for the relation between the spectral index and the redshift and/or low-frequency radio luminosity:

1. *K*-Correction

Since observed radio spectra tend to steepen with increasing frequency, the *K*-correction of such curvature will lead to a correlation of spectral index with redshift. Blumenthal and Miley (1979) considered this effect but concluded that it was unlikely to explain in full the observed relation between spectral index and redshift. See also Gopal-Krishna (1988) and Laing and Peacock (1980). In the case of 4C 41.17, the steep spectrum is straight and appears to continue to as low an observed frequency as 26 MHz (see Fig. 6) demonstrating that the *K*-correction does little to steepen the observed spectrum.

2. Injection

The details of the supply of the relativistic electrons may be important. A simple model which may have some application here is the well-known case considered by Kardashev (1962) in which there is continuous replenishment of newly accelerated electrons. Such a model has been applied to many sources, including ultrasteep spectrum sources and Cygnus A hot spots (e.g., Roland *et al.* 1982; Roland *et al.* 1985; Eales, Alexander, and Duncan 1989). We begin by considering the hot spot as a leaky reservoir into which relativistic electrons are injected and remain for a time τ_{inj} after which they diffuse into the lobes. In this situation, the resultant spectrum should consist of three distinct spectral regions with indices α_0, $\alpha_1 = \alpha_0 - \frac{1}{2}$, and $\alpha_2 = (4/3)\alpha_0 - 1$ (see Fig. 9). In the first spectral region, the synchrotron radiation losses are unimportant and the spectrum has a "normal" spectral index α_0. In the second region, the time scale for radiation losses τ_{rad}, is longer than the period τ_{inj} between bursts, and the injection can be considered quasi-continuous. The spectrum is in equilibrium since radiation losses are balanced by the injection of new particles. The break between the first and second regions occurs at a frequency $\nu_{12} \sim B^{-3}\tau_{rad}^{-2}$ GHz and that between the second and third regions occurs at $\nu_{23} \sim B^{-3}\tau_{inj}^{-2}$ GHz, where B is in G and τ is in yr. Note that the total radio luminosity $L_{tot} \propto B^{7/2}$, and therefore more luminous sources of the same volume and injection time scale will have the steeper regions of the Kardashev spectrum at lower frequencies.

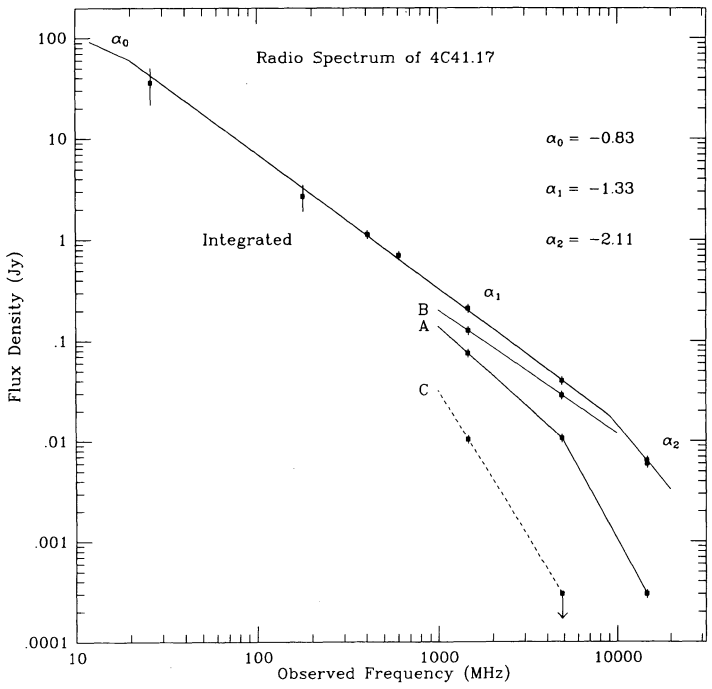

FIG. 9.—Radio spectrum of 4C 41.17. Integrated spectrum and spectra of individual components. The spectral indices and breaks are discussed in the text.

The observed spectrum of 4C 41.17 (Fig. 9) implies that the first spectral break occurs at an observing frequency of less than about 40 MHz (188 MHz, rest frame). Substituting the equipartition magnetic field strengths, we obtain that $\tau_{rad} \sim 9 \times 10^5$ yr.

At frequencies between 4.8 and 14 GHz the integrated spectrum of 4C 41.17 does steepen. At 14 GHz (67 GHz rest frame), we may be observing the exponential cutoff where the spectrum is dominated by synchrotron radiation losses. This break suggests a period $\tau_{inj} \sim 5 \times 10^4$ yr for bursts of newly accelerated particles. In this picture the radiative lifetimes given in Table 4, based on the largest observed frequency, would still represent the maximum age of the most recently accelerated electrons. Component *B* contributes most of the flux at 14 GHz and may not be steepening. However, the extreme spectrum of component *C*, observed only at 1.4 GHz (6.7 GHz rest frame), could indicate that the particle supply to this feature has ceased and that the resultant radiation will only continue for another $\sim 10^5$ yr.

3. Other

Other processes may well be involved in producing the ultrasteep spectrum. For example, Pelletier and Roland (1988) have suggested a theory of mixed shocks where steep spectrum hot spots can be produced by jets with a magnetic field parallel to the jet.

b) The Optical/Infrared Continuum

i) *Nature of the Radiation*

Is the optical and infrared emission from 4C 41.17 dominated by starlight, i.e., is 4C 41.17 a galaxy? Stimulated by the discovery of the alignment effect, various alternative mechanisms have been proposed for the origin of the continuum emission in high-redshift radio galaxies; e.g., gravitational lensing, nonthermal emission, and scattering of nonthermal radiation from the active nucleus (Le Fèvre and Hammer 1988; Fabian 1989; di Serego Alighieri *et al.* 1989; Tadhunter *et al.* 1989; Eales and Rawlings 1990; Scarrott, Rolph, and Tadhunter 1990). These various alternative explanations for the optical/IR continuum from distant radio galaxies have been reviewed by Chambers and Miley (1989).

However, there is some direct evidence, in the form of ultraviolet stellar absorption features, that the extended continuum from high-redshift radio galaxies is due to stars (Chambers and McCarthy 1990). In the case of 4C 41.17, evidence for stellar emission includes the following:

1. The resemblance of the SED of 4C 41.17 (Fig. 7) to that of a galaxian spectral energy distribution.

2. The evidence for a "1500 Å break" which is difficult to obtain in nonthermal scenarios but is a natural consequence of a stellar population with a decreasing star formation rate (Chambers and McCarthy 1990).

3. The decrease in continuum flux shortward of Lyα is consistent with the drop that would be expected from a stellar continuum and at the 1 σ level is more than the factor of 3 expected from the Lyα forest at this redshift.

4. The C IV/Lyα ratio (0.1) of 4C 41.17 which is comparable with those of other powerful radio galaxies, but is much lower than those observed in high-redshift quasars, even those with narrow lines (Foltz *et al.* 1983).

In sum, all the observed properties of 4C 41.17—radio, optical, and line emission—are similar to those of other high-redshift radio galaxies (e.g., Spinrad 1986), in which most of the light appears to be starlight (Chambers and McCarthy 1990). Therefore we will proceed with our discussion of 4C 41.17 on the working assumption that while there may exist contributions from other mechanisms (e.g., a dust-scattered nonthermal component in the blue), most of the extended continuum emission from 4C 41.17 is from stars. At a redshift of 3.8, 4C 41.17 is therefore the most distant stellar system presently known.

ii) *Constraints on the Stellar Composition*

At a redshift of 3.8, it is important to investigate the stellar composition of 4C 41.17 in an attempt to obtain some information about the formation and evolutionary history of at least one galaxy at such an early epoch regardless of how typical it is. In particular, the ages of the stellar population relative to that of the radio source and the mass involved in stars are crucial in investigating whether, as has been proposed, star formation in high-redshift radio galaxies is induced by the propagation of the radio source (Chambers, Miley, and van Breugel 1987; McCarthy *et al.* 1987*b*). We have therefore attempted to fit the spectral energy distribution (SED) of 4C 41.17 (Fig. 6) to some representative models of synthetic stellar populations using an updated version of Bruzual's code (1983). (See also Chambers and Charlot 1990). In the spectral range of interest, the stellar spectra used in the model are from the *OAO* and *IUE* observations. All tracks and spectra are for solar metallicity only. The models presented below are computed with a Scalo (1986) initial mass function (IMF) with a lower and upper cutoffs of 0.08 and 75 $M_\odot$, respectively. Four models were considered. The first considers an old stellar component, comparable to the model of Lilly (1988). The other three correspond to star formation taking place over time scales comparable with the likely radio age ($\sim 10^8$ yr). The SED in Figure 7 was fitted by eye for each model and various optimum model parameters are tabulated in Table 6. Three of these parameters are of particular interest in comparing the models: (1) the "persistence" of the observed SED defined as the length of time during its evolution that a galaxy has colors consistent (to a factor of 2 in relative flux) with the observed SED; (2) the "fractional age," defined as the persistence divided by the total age of the galaxy; and (3) the "fractional luminosity" defined as the ratio of the luminosity of the observed SED to the peak luminosity required by that model. We stress that these models are not unique; however, they are useful in examining which scenarios are consistent with the data, and which are not.

1. Model A: Old + Burst

Lilly (1988, 1989*b*) has argued that the red bump is due to an older stellar component and the blue light is due to a second recent burst of star formation. For this model we assume that the bulk of the stars are formed in a continuous burst lasting 1 Gyr. Then the star formation halts and the population evolves. By itself, this is equivalent to a Bruzual "c" model. However, at some later epoch (the epoch of observation) a second starburst is added (possibly associated with the radio activity). This second burst is responsible for the flat ultraviolet component, and its high star formation rate need only last for a short period of time. We find that the older generation had to be at least 1.3 Gyr old, but to get the best fit in the ultraviolet, even the burst has to evolve (see Chambers and McCarthy 1990), and hence the best fit minimum age is 1.5 Gyr. The young starburst is taken to be a constant burst lasting 0.1 Gyr with a mass fraction of 0.04 of the original burst. (For discussion of a similar model, see also Rocca-Volmerange 1989, and Rocca-Volmerange and Guiderdoni 1989.)

TABLE 6

SAMPLE MODELS OF THE STELLAR POPULATION IN 4C 41.17

PARAMETER	NAME/MODEL			
	Old + Burst/A[a]	Massive Stars/B[b]	Young/C[c]	Young + Dust/D[d]
Age of galaxy (Myr)	1600	180	300	100
Persistence of observed SED (Myr)	100	5	80	100
Fractional age of SED	0.06	0.03	0.33	1.0
Time since peak luminosity (Myr)	500	180	270	0
(Luminosity of SED)/(peak Luminosity)	0.53	0.04	0.24	1.0
Current SFR ($M_\odot$ yr^{-1})	350	0	110	4300
Equivalent width Lyα emission line (Å)	240	abs.	140	abs.
Equivalent width Lyα at peak (Å)	240	300	390	400
Mass in stars (10^{11} $M_\odot$)	11	0.21	5.5	5.2
Number of stars (10^{11})	25	0.042	1.2	11
M/L (only objects in IMF)	0.6	0.0045	0.30	(0.06)[e]
Fraction low-mass giants ($M < 1.8\ M_\odot$)	0.0016	0	0	0
SNR yr^{-1} (rest frame)	2.5	0.02	5	25
Average mass of luminosity star ($M_\odot$)	8.5	5	4.8	18
Average luminosity of star ($L_\odot$)	0.8	1100	1.6	8.7
Extinction A_{BV} (SMC curve)	0	0	0	0.8
M_{BOL}	−26.03	−26.94	−25.95	(−27.74)[e]
M_V (rest frame)	−25.39	−25.85	−2539	(−25.26)[e]
M_K (rest frame)	−27.26	−29.01	−27.39	(−28.36)[e]

[a] SFR: $(c = 1) + 0.04\,(c = 0.1)$; IMF: S calo.
[b] SFR: $c = 0.1$; IMF: $x = 1.35$, $M > 5\ M_\odot$.
[c] SFR: $\tau = 0.07$; IMF: S calo.
[d] SFR: $c = 0.1$; IMF: S calo.
[e] Unreddened values.

There are two major difficulties with this old stellar population model:

1. The large ages asserted for the highest redshift objects become a powerful constraint on the epoch of formation of these galaxies and on cosmological models as well. If 4C 41.17 is older than $\sim 1.3 \times 10^9$ yr, then this excludes an $H_0 = 50$, $q_0 = 0.5$ cosmology where the universe is only 1.28×10^9 yr old at a redshift of 3.8. While the problem is not as extreme for low-q_0 cosmologies, large ages for the highest redshift radio galaxies imply very high redshifts of formation $z_F \sim 10$–30.

2. The most crucial objection is that old stellar population model cannot explain the infrared alignments seen in 4C 41.17 and in high-redshift radio galaxies in general (Chambers, Miley, and Joyce 1988; Eisenhardt and Chokshi 1990). Since the ages of the galaxies in this model are far larger than is reasonable for the radio source, one is forced to argue for some sort of star formation along the radio axis giving rise to the blue alignments, and an additional ad hoc mechanism at work for the infrared alignments.

2. Model B: Massive Stars

Using an IMF restricted to massive stars is an efficient way to produce a large luminosity with relatively few stars over a relatively short period of time. However, it is difficult to produce a plausible massive star scenario that fits the spectral energy distribution since massive stars spend more time being blue than red. Several models with an IMF (Salpeter slope of 2.35) truncated to contain only massive stars and different prescriptions for the star formation rate were investigated with the following results:

1. No steady state model was found that could satisfactorily fit the red bump.

2. An evolving model with an exponentially decaying star formation rate evolves quickly until it reaches a steady shape which depends entirely on the (arbitrarily chosen) lower mass cutoff. For all exponential models tried, this shape was too blue to match the SED of 4C 41.17. The reddest SED obtained occurred after the total luminosity had decreased by a factor of ~ 0.003.

3. An evolving model with a constant burst of star formation lasting 1×10^8 yr, followed by simple evolution, was capable of matching the observations of 4C 41.17. Models with lower limits between 5 and 8 $M_\odot$ could fit the data, but the 8 $M_\odot$ is uncomfortably red at longer wavelengths. See Bithell and Rees (1989) for discussion of a similar model.

There are several difficulties with the massive star models:

1. The massive star model could not be fitted without invoking a very small fractional age, i.e., the model SEDs fitted the data only for a very small percentage of its luminous phase, spending a much greater fraction of its lifetime ($\sim 90\%$) with a very blue SED, or being extremely red ($\sim 5\%$ of its luminous lifetime). Using this model, it would therefore be difficult to explain why many high-redshift radio galaxies have similar SEDs to 4C 41.17.

2. The very small fractional luminosity requires that these objects be ~ 25 times more luminous (or 3.5 mag) brighter at their peak peak than they are now. Since aligned radio galaxies are already very luminous, such a model would predict extreme luminosities for their burst phase.

3. Because the massive star model evolves so quickly it is difficult to explain the observed continuity and low dispersion of the infrared Hubble diagram for high-redshift radio galaxies (Lilly 1989*b*).

4. Although the "ad hoc" nature of the lower mass cutoff (~ 5 $M_\odot$) is artificial, this cutoff determines all the relevant properties of the model.

Hence, we regard it unlikely that a massive IMF alone can account for the stellar composition.

3. Model C: Young Stellar Population

This is a short but powerful burst of star formation with an exponential decline of the form $\psi(t, \tau) = (M_g/\tau)e(-t/\tau)$, where M_g is the total mass of galaxy, t is its age, and τ is the characteristic time for star formation. This expression for the star formation rate is comparable to that of a Bruzual "μ" model, but with $\tau = 7 \times 10^7$ yr. Such a time scale is comparable to a free fall time and is reasonably well matched to the likely age of the radio source. The evolution of this model produces a "red bump + flat UV" SED that matches the 4C 41.17 in a galaxy age of about 3×10^8 yr.

This model is comparable to, although somewhat simpler than, the model of Chambers and Charlot (1990). They showed that the observed SEDs of high-redshift radio galaxies (0902+34 and 4C 41.17 in particular) can be produced with a normal (Scalo 1986) IMF in less than $\sim 3 \times 10^8$ yr if the galaxies formed the bulk of their stars on slightly shorter time scales ($\lesssim 1 \times 10^8$ yr). This suggests that these objects could be relatively young and that we are observing them (at least the ones with the flat UV) near the time in which they formed most of their stars. The "epoch" of this type of galaxy formation would have extended over a fairly wide range of redshifts, from $z \sim 1$ to $z \sim 5$. Therefore the large ages suggested by Lilly (1988) are not required.

The ability to obtain "flat UV plus red bump" SEDs on short time scales and maintain a roughly constant red luminosity during the first Gyr of the life of the galaxy makes the young galaxy scenario (Chambers and Charlot 1990) the only model so far capable of explaining both the infrared alignments while at the same time maintaining the observed small dispersion and continuity of the Hubble diagram.

This model is also similar to that used by Chambers and McCarthy (1990) to model the stellar absorption features and the "1500 Å break." The amount of past star formation required to match the "1500 Å break" is in excellent agreement with that required to produce the "red bump" on a short time scale.

4. Model D: Young Stars plus Dust

This model assumes that we are observing a constant rate of star formation but that the SED is reddened due to the presence of dust, having an extinction curve derived from the Small Magellanic Clouds (Prévot *et al.* 1984). A Galactic extinction curve (Savage and Mathis 1979) would introduce a strong feature at 2200 Å. The model assumes a constant rate of star formation lasting for 1.0×10^8 yr, although due to the constant star formation the SED is not sensitive to the age of the model.

This ad hoc model uses the dust extinction as a free parameter to fit the data. Although polarization measurements of the blue light in 3C 368 may indicate the presence of a limited amount of dust (di Serego Alighieri *et al.* 1989 and Scarrott, Rolph, and Tadhunter 1990), high-redshift radio galaxies are not expected to contain much dust because of their large Lyα surface brightnesses. Even a small amount of dust can extinguish most resonance line photons such as Lyα. However, the dust could be clumped differently from the emission line gas. Dust would mainly affect the rest frame "flat UV" part of

the spectrum but hardly affect the red or near-infrared emission. Thus if dust is present in large amounts in these objects, it would not change the basic conclusions of the young galaxy picture discussed above. The greatest affect of ignoring reddening would be to *overestimate* the ages derived from the observed SEDs.

5. Summary

The young galaxy model discussed provides a good fit to the observations of 4C 41.17 and provides the best explanation for the properties of high-redshift radio galaxies in general (e.g., Chambers and Miley 1989; Chambers and Charlot 1990; Chambers and McCarthy 1990). However, a consequence of this conclusion is that powerful radio sources like 4C 41.17 must be capable of stimulating substantial star formation at high redshift.

iii) *Plausibility of Radio Source–induced Star Formation*

Can a radio source trigger vast amounts of star formation at early epochs? Various approaches have been discussed by Rees (1989), Begelman and Cioffi (1989), De Young (1989), and Daly (1990). Certainly protogalaxies present an ideal environment for radio source–induced star formation since a two-phase medium of hot gas and cold dense clouds is a nearly inevitable consequence of inhomogeneities during collapse (Fall and Rees 1985). Infalling material is heated to the virial temperature, 10^6–10^7 K, with embedded clouds or filaments at $\lesssim 10^4$ K. If the cocoons of shocked gas that are expected to surround powerful radio sources (Scheuer 1974) engulf and compress these protogalactic clouds, this may drive them over the Jeans limit and trigger star formation. Rees (1989) estimates that the star formation rate can be enhanced by the radio source over what one would otherwise expect from normal gasdynamical considerations (e.g., Fall and Rees 1985) by an amount comparable to the Mach number of the radio jet, i.e., by a factor of $\sim$10–100. This suggests a dramatic star formation rate, and if the cocoon engulfs the entire protogalaxy then the formation of the galaxy (conversion of gas to stars) might occur $\sim$10–100 times faster.

In order to calculate the pressure p_c and age t of the cocoon of 4C 41.17 using the expressions of Begelman and Cioffi (1989) we require estimates of the power L_j, velocity v_j, and Lorentz factor γ of the jet, the dimensions of the cocoon (width w_c and length l_c) and the bow shock (cross sectional area A_h) and the electron density $n_{e,\rm hot}$ of the hot phase ambient medium. Note that we assume Scheuer's (1982) suggestion that the jet direction fluctuates on a time scale short compared to the evolution of the cocoon; therefore, the average momentum flux of the radio jet is spread out over a much larger area than the instantaneous cross section of the jet. The velocity of the advance of the bow shock can therefore be much smaller than the velocity of the jet.

We can make three estimates of the jet power in 4C 41.17:

1. The jet thrust for a high Mach number jet $\Pi_j = L_j(\gamma + 1)/(v_j\gamma)$ (Bridle and Perley 1984) can be computed from the minimum pressure and the area of the "B_3" hot spot, giving $\lesssim 10^{36}$ dyn. Since 4C 41.17 has a total radio luminosity comparable to or greater than Cygnus A, we will assume similar parameters for jet, and thus $\gamma \sim 1.6$ and $v_j \sim c$ (e.g., Perley, Dreher, and Cowan 1984, but see also Roland, Pelletier, and Muxlow 1988). The resulting jet power for 4C 41.17 is $\sim 3.0 \times 10^{46}$ ergs s^{-1}.

2. From the arguments in § IV*a* the minimum energy in the unresolved hot spot must be replenished on a time scale $\tau_{\rm inj} = 2 \times 10^3$ yr, or a jet power of $\sim 7 \times 10^{46}$ ergs s^{-1}.

3. A jet power of $(10^{46}/2\epsilon)$ is obtained from the total radio luminosity, where ϵ is the conversion efficiency factor and is probably on the order of 0.1–0.01. Therefore a jet power of $\gtrsim 10^{46}$ ergs s^{-1} for 4C 41.17 is a reasonable assumption.

The cocoon itself is not observed; its existence is inferred by standard arguments requiring the accumulation of "waste energy" (Scheuer 1974). However, it is expected to be somewhat longer than the largest angular size of the radio source with the width a factor of $\sim$0.1–1.0 of the length. Thus it is interesting to speculate that the Lyα "halo" (§ III*d* and Fig. 6*c*) which is elliptical in shape and well aligned with the radio source may trace the extent of the radio cocoon. If the star formation is driven by the radio cocoon, one would expect Lyα emission from the cocoon. This might account for the overall morphology and orientation of the Lyα halo. For this discussion we will therefore take the cocoon to have the dimensions of the Lyα halo ($\gtrsim 18'' \times \gtrsim 10''$).

There are no prospects of direct radio observations of the bow shock in 4C 41.17; to date the only observation of a hot spot working against a large bow shock is that of Cygnus A (Carilli, Perley, and Dreher 1988; compare with 3C 33, Rudnik 1988). However, as with the cocoon, there are features in the Lyα emission that are reminiscent of a bow shock (Figs. 6*b* and 6*c*). Within the "galaxy" component we note the bow-shaped feature in the Lyα galaxy component, extending from the hotspot B_3 backward (westward) along the sides of the lobe. If this line emission is associated with the bow shock, then it is larger ($A_h \gtrsim 100$ kpc^2) than in Cygnus A ($A_h \sim 30$ kpc^2; Carilli, Perley, and Dreher 1988). The larger bow shock in 4C 41.17 may be attributed to the propagation of the jet into a denser medium in the high-redshift galaxy.

From Table 3 we use the estimate for the ambient density required to confine the radio source with a ram velocity of $\sim$1000 km s^{-1}. Taking the value derived from the integrated values for B_{23} gives $n_{e,\rm hot} \sim 0.2$ cm^{-3}, but it may be as high as ~ 10 cm^{-3}, as indicated from the estimates of the unresolved flux.

We can now use the expression from Begelman and Cioffi (1989) to estimate the pressure in the cocoon of 4C 41.17 using the above estimates for the physical parameters,

$$p_c = 3.8 \times 10^{-9} \text{ dyn cm}^{-2} \times L_{j,46}^{1/2} n_{e,\rm hot}^{1/2} \beta_j^{1/2} A_{h,28}^{1/2} l_{c,50}^{-2} \left(\frac{l_c}{w_c}\right)^2 , \quad (1)$$

where $L_{j,46}$ is the jet luminosity in 10^{46} ergs s^{-1}, β_j is the velocity of the jet, and $A_{h,28}$ is the area of the bow shock in 28 kpc^2. For $l_c/w_c \sim 1.5$ and $n_e \sim 0.2$ the pressure in the cocoon is $\sim 4 \times 10^{-9}$ dyn cm^{-2}, consistent with the pressures and densities indicated by the Lyα measurements (Table 5).

Similarly a minimum estimate of the age of the cocoon is

$$t = 1.4 \times 10^8 \text{ yr } L_{j,46}^{-1/4} n_{e,\rm hot}^{1/4} \beta_j^{-1/4} A_{h,28}^{-1/4} l_{c,50}^2 \left(\frac{l_c}{w_c}\right)^{-2} . \quad (2)$$

For the above parameters this is $\sim 3 \times 10^7$ yr. Combining this with the observed source size gives velocities of $\sim$1000 km s^{-1}, consistent with the maximum velocities observed for the gas. However, from the existence of lobe "*C*," the radio source has been both larger and redirected in the past; hence, the age of the cocoon may be significantly larger than this estimate. Fur-

thermore the higher density indicated by the unresolved radio flux (Table 4) would give an age of $\sim 1.1 \times 10^8$ yr.

Next we enquire whether such a process could result in a star formation rate which is large enough and of a suitable form to account for the observed spectral energy distribution of 4C 41.17. In order for the cocoon to stimulate the bulk of the star formation of the galaxy it must have engulfed the volume of the galaxy. On 4C 41.17 the extended continuum emission, and thus the galaxy, extends along the radio axis even *beyond* the eastern lobe "B_3." However, this is plausible in Scheuer's (1982) "Dentist Drill" model wherein the jet direction fluctuates on a time scale short compared to the evolution of the cocoon. The existence and extremely steep radio spectrum of the easternmost lobe "C" implies that the jet of 4C 41.17 has extended eastward beyond "B_3" in the recent past and thus the cocoon extends beyond lobe "B_3," and may form stars beyond the apparent instantaneous working surface of the jet. Certainly if the Lyα halo is tracing the cocoon then the cocoon extends well beyond lobe "B_3." Therefore the premise is that the cocoon has engulfed the volume of the protogalaxy, the mass converted into stars would be

$$M_{\rm stars} = 3.4 \times 10^{11}\, M_\odot \left(\frac{V}{10^{70}\ {\rm cm}^3}\right)\left(\frac{f_{\rm proto}\epsilon}{10^{-4}}\right) \times \left(\frac{\rho_{\rm cold}}{7 \times 10^{-22}\ {\rm g\ cm}^{-3}}\right), \quad (3)$$

where $V \lesssim V_{\rm cocoon}$ is the volume of the protogalaxy, $f_{\rm proto}$ is the preformation filling factor of the dense clouds, ϵ is the efficiency of conversion of gas into stars, and the estimate of $\rho_{\rm cold} = (\mu_c T_h/\mu_h T_c)\rho_{\rm hot}$ in a protogalactic environment is from Fall and Rees (1985). For an initial filling factor of $f_{\rm proto} \sim 10^{-3}$ and star formation efficiencies of $\sim 10\%$, this will form the bulk of the galaxy in lifetime of the cocoon ($\lesssim 3 \times 10^8$ yr) with a star formation rate of $\gtrsim 1000\ M_\odot\ {\rm yr}^{-1}$. This is in reasonable agreement with the star formation rate in model C above and in Chambers and Charlot (1990).

Such an enormous peak star formation rate is admittedly very high, but it is not extreme in the context of other high-redshift radio galaxies. Lilly (1988) estimates the current star formation rate in 0902+34 is $\sim 100\ M_\odot\ {\rm yr}^{-1}$, similar to our estimate for the current star formation rate in 4C 41.17. As discussed above he also concluded, on the basis of continuum data, that there must have been a much higher peak star formation rate at a much earlier epoch. McCarthy *et al.* (1987*a*) estimated a star formation rate of $\sim 500\ M_\odot\ {\rm yr}^{-1}$ in 3C 326.1, assuming that all the Lyα flux came from star formation. While this is probably not the case, some of their arguments for the plausibility of high peak star formation rates apply. For instance, given the very large volume over which star formation is taking place, the star formation rate per volume is less than that of starburst nuclei.

The continuing but decreasing star formation rate may in part be due to secondary processes occurring after the passage of the cocoon shock, e.g. supernovae driven shocks. The color gradients described in § III*c* and Figure 5*b* show a trend toward bluer colors eastward along the radio axis. This may be due to a trend in the star formation rate that propagates along the axis with the radio source. Note the overall efficiency could be lower if the volume or filling factor were larger, but a high efficiency in the star-forming episode of giant ellipticals is plausible.

We conclude that our radio, optical/IR continuum, and Lyman-alpha observations of 4C 41.17 are all consistent with a picture in which the bulk of the galaxy forms by star formation induced by the radio source.

c) The Lyman-α Gas

In § III*d* we found that the emission-line gas associated with 4C 41.17 has several distinct morphological and kinematical components we called the jet, galaxy, halo, and disk. We now examine the kinematics and ionization of each of these components.

i) *Kinematics*

1. Interaction with the Radio Jet and Entrainment

There are several arguments suggesting that the high-velocity line-emitting gas we call the "jet" is kinematically interacting with the radio source:

1. The high velocity gas is extended over at least 5″ or 35 kpc and spatially correlated with the radio source.
2. The kinematic energy of the gas is considerably less than the minimum energy requirements of the radio source.
3. There is previous evidence that radio sources can entrain and accelerate gas (e.g., De Young 1981; van Breugel *et al.* 1985*b*).

To quantify the entrainment we use the "two-process" formulation of De Young (1986). The first "prompt" process is a rapid entrainment at the head of the jet by the bow shock associated with the hot spot, and the second "steady state" process is associated with the boundary layer between the outbound jet and the medium. We may be observing both processes in 4C 41.17 where one natural explanation for the peak in the Lyα at the leading edge of the easternmost hot spot "B_3" is due to entrainment at the bow shock.

From De Young (1986) the prompt process entrainment rate at the bow shock is

$$\dot{M}_p = 375\ M_\odot\ {\rm yr}^{-1}\ n_{e,\rm hot}\, v_{h,8}\, A_{e,28}\ , \quad (4)$$

where $v_{h,8}$ is the effective velocity of the head or bow shock in 10^8 cm s^{-1} and A_e is the *effective* entrainment area of the bow shock. If $A_e = A_h$, this results in a total entrained mass of $\sim 7.5 \times 10^9\ M_\odot$ in 10^8 yr. Comparing with the mass estimates from the Lyα emission in Table 5, this suggests that a reasonable fraction of the line-emitting gas at B_3 was entrained and accelerated by the bow shock if the efficiency of entrainment at the bow shock is $\gtrsim 1\%$.

Entrainment behind the bow shock is more uncertain, particularly if the jet is moving at bulk relativistic velocities. However, we can make a rough estimate of the mass entrained using De Young's (1986) expression for the steady state mass entrainment rate for a nonrelativistic jet:

$$\dot{M}_{\rm ss} = 4.6\ M_\odot\ {\rm yr}^{-1}\ R_b^{-1} n_{e,\rm hot}\, v_{b,8}\, R_{b,\rm kpc}^2\, \epsilon\ , \quad (5)$$

where R_b is the radius of the jet, $v_{b,8}$ is the velocity of the jet in 10^8 cm s^{-1}, and ϵ is the efficiency factor. On the assumption that the turbulent boundary layer penetrates to half the jet radius, the efficiency factor $\epsilon \sim 0.3$ for a high Mach number jet, and a 1 kpc radius (De Young 1986), the mass entrainment is $\sim 15\ M_\odot\ {\rm yr}^{-1}$. Over a radio source lifetime of 10^8 yr the entrained mass would be $\sim 10^9\ M_\odot$ or $\sim$2–10 times the mass in the Lyα emission-line gas (Table 5). If such entrainment of the gas by the jet was occurring, one might expect the velocity of the gas to increase systematically along the jet as it is accelerated to the jet speed. That is consistent with the velocity field shown in Figure 5.

In this context it is interesting to consider the wiggle in the gas morphology (Fig. 6) discussed in § III*d*. It is suggestive that the length scale of the wiggle is comparable with that of the radio component separation, and the position angle variation of the wiggle is comparable with the position angle difference between the inner and outer radio structures. For these reasons it is tempting to associate the wiggling in the Lyα image with entrainment of the gas by the radio source coupled with precession of the radio source axis. The wiggle length scale (3 kpc) coupled with the gas velocity (1000 km s^{-1}) would then imply a time scale of about 3×10^6 yr for the precession of the radio source.

2. Gravitational Dynamics

Although the passage of the radio cocoon will transfer some momentum to the emission-line clouds, once the shock has passed the kinematics of the remaining components—galaxy, halo, and disk—are unaffected by the radio source and will be dominated by gravity. The "disk" feature discerned in the kinematic data (§ III*d*) may be a coincidence of a systematic velocity component in the jet and a unassociated extended cloud. However, if it is a coherent structure, and its kinematics are driven by gravity, then with an apparent circular velocity of ~ 120 km s^{-1} out to ~ 100 kpc, this indicates an interior mass for the disk of $\sim 3 \times 10^{11} \sin^2(i)\, M_\odot$ but shifted 500 km s^{-1} relative to the peak in the Lyα.

If component "v" at a distance of 10″ is not related to the jet, but is in circular motion about the galaxy as part of the halo, this indicates an interior mass of $\sim 3 \times 10^{12} \sin^2(i)\, M_\odot$.

ii) *Ionization*

What is responsible for ionizing the Lyman-alpha gas? The answer to this question must account for the alignment between the various components of the ionized gas and the radio axis. Similar cases of morphologically associated radio continuum and optical line emission are seen in the majority of radio galaxies at lower redshifts ($z < 0.2$, Baum *et al.* 1988; $0.5 < z < 1.8$, McCarthy *et al.* 1987*b*). The ionization processes involved in 4C 41.17 may be similar; however, it is important to note the additional ingredient of the optical and infrared continuum alignment with the radio source in the high-redshift radio galaxies. Therefore, we discuss three main possibilities for contributors to the ionization:

1. Ionization by Stellar Photospheres

The stellar population models used to fit the observed spectral energy distribution (§ IV*b*) produce enough ionizing photons from stars to account for about two-thirds of the observed Lyα equivalent width. Assuming 100% of the ionizing photons are converted into Lyα photons model C produces an equivalent width of 138 Å. This should be compared with a rest frame equivalent width for the galaxy component of $\sim 1000/(1+z) = 208$ Å. The Scalo IMF used extends up to 70 $M_\odot$; if there were more massive stars, the ionizing continuum from stars would increase. Thus it is possible that all of the Lyα could be accounted for by stellar photospheres, but a conservative estimate is that half of the ionizing photons come from the observed extended emission.

2. Anisotropic Ionizing Continuum from the Nucleus

There is increasing evidence that some extended emission line regions in low-redshift radio galaxies is due to ionizing photons escaping preferentially along the radio axes (e.g., Danzinger *et al.* 1984; Fosbury, Tadhunter, and Danzinger 1984; Baum and Heckman 1989*a*, *b*). Anisotropic radiation of the nuclear continuum from active galaxies has been discussed extensively (e.g., Steiner 1981; Antonucci 1984, 1987; Unger *et al.* 1987; Baum and Heckman 1989*a*, *b*; Tadhunter 1989). One hypothesis is that the anisotropy is due to an optically thick torus surrounding the nuclear region has received particular attention as part of a "unified" scheme for QSOs and radio galaxies (Barthel 1989). In the case of 4C 41.17, anisotropic nuclear photoionization would provide a natural explanation for the presence of the Lyα halo as well as the bright "jet" feature which extends eastward beyond the radio lobes in a direct line with the "*B*" radio lobes. There is, however, no indication of an "inverted cone" structure in the Lyα halo like those seen in low-redshift examples of anisotropic ionization (Fosbury, Tadhunter, and Danzinger 1984), i.e., there seem to be plenty of ionizing photons along the minor axis. However, some nonthermal continuum is required to account for the C IV high-ionization line.

3. Ionization by the Radio Jet

As discussed in the previous section, the Lyα halo may well trace the cocoon presumed to surround the radio source. The radio jet and the associated cocoon must generate shocks as they propagate outward into the ambient medium. These shocks can contribute to ionizing the gas, either directly by collisional excitation or by producing X-rays which would be a source of photoionization (e.g., Heckman *et al.* 1982; Baum and Heckman 1989*a*, *b*).

V. CONCLUSIONS

There are several conclusions that we can draw from the large body of data that we have presented here:

1. 4C 41.17 is associated with an extended source of optical and infrared emission, most likely dominated by starlight, at a redshift of 3.8. It is therefore the most distant stellar system presently known.

2. The morphological similarities between the ionized gas, the optical/infrared continua and the radio source indicate that the radio source is interacting vigorously with the galaxy.

3. The spectral energy distribution is consistent with a stellar synthesis model for the galaxy in which the bulk of the stars formed in $\lesssim 10^8$ yr, and the galaxy is now $\lesssim 3 \times 10^8$ yr old. This star formation rate could have been produced by the overpressurized cocoon of the radio source compressing protogalactic clouds over their Jeans limit. In this manner it is plausible that the radio source stimulated the formation of $\sim 10^{11}$–$10^{12}\, M_\odot$ of stars with a normal (Scalo) IMF.

4. 4C 41.17 possesses a luminous ($\gtrsim 10^{44}$ ergs s^{-1}) giant ($\gtrsim 100$ kpc) clumpy Lyα halo. Several processes can contribute to ionizing the line-emitting gas. These include photoionization by young stars (could account for about 0.66 of the luminosity), shocks induced by interaction with the radio source, or anisotropic photoionization by nuclear (continuum) emission.

The Lyα and radio emission from 4C 41.17 could easily be detected out to a redshift of 6, beyond which the line would be shifted outside optically observable wavelengths. Extension of our search technique to fainter samples of sources promises to increase the numbers of known high-redshift radio galaxies considerably and provide large numbers of unique probes of the early universe. We have begun a program to do this.

We are grateful for the detailed comments on the paper by Tim Heckman and Hy Spinrad, and to Mike Fall, Colin Norman, Peter Quinn, and Joe Silk for stimulating discussions

about the "nature of the beast." We thank Gustavo Bruzual for allowing us to use his code, and to Stéphane Charlot for help in using the code. We appreciate the assistance of the staffs of KPNO and the VLA. Joel Alcock and Delores Walker gave assistance at UKIRT and Simon Lilly and Ian McLean gave us useful advice on the infrared observing techniques. Jeannette Barnes provided invaluable assistance with IRAF. Jim Condon provided help with the NRAO Computer Assisted Astrometry System. K. C. C. thanks Arthur Davidsen and the Hopkins Ultraviolet Telescope Project, NASA contract NAS 5-27000, for partial support. W. v B. acknowledges partial support from NSF grant AST 84-16177. G. K. M. and K. C. C. acknowledge partial support from a NATO research grant.

REFERENCES

Antonucci, R. R. J. 1984, *Ap. J.*, **278**, 499.
Antonucci, R. R. J., Hickson, P., Miller, J. S., and Olszewski, E. W. 1987, *A.J.*, **93**, 785.
Allington-Smith, J. R. 1982, *M.N.R.A.S.*, **199**, 611.
Barthel, P. D. 1989, *Ap. J.*, **336**, 606.
Baum, S. A., Heckman, T. M., Bridle, A., van Breugel, W. J. M., and Miley, G. K. 1988, *Ap. J. Suppl.*, **68**, 833.
Baum, S. A., and Heckman, T. M. 1989*a*, *Ap. J.*, **336**, 681.
———. 1989*b*, *Ap. J.*, **336**, 702.
Begelman, M. C., and Cioffi, D. F. 1989, *Ap. J. (Letters)*, **345**, L21.
Bennet, A. S. 1962, *M.N.R.A.S.*, **68**, 163.
Bithell, M., and Rees, M. 1990, *M.N.R.A.S.*, **242**, 570.
Blumenthal, G., and Miley, G. K. 1979, *Astr. Ap.*, **80**, 13.
Bridle, A. H., and Perley, R. A. 1984, *Ann. Rev. Astr. Ap.*, **22**, 319.
Bruzual, G. 1983, *Ap. J.*, **273**, 105.
Burstein, D., and Heiles, C. 1982, *A.J.*, **87**, 1165.
Carrilli, C. L., Perley, R. A., and Dreher, J. H. 1988, *Ap. J. (Letters)*, **334**, L73.
Chambers, K. C. 1989, Ph.D. thesis, The Johns Hopkins University.
Chambers, K. C., and Charlot, S. 1990, *Ap. J. (Letters)*, **348**, L1.
Chambers, K. C., and McCarthy, P. J. 1990, *Ap. J. (Letters)*, **354**, L9.
Chambers, K. C., and Miley, G. K. 1989, in *The Evolution of the Universe of Galaxies: The Edwin Hubble Centenial Symposium*, ed. R. G. Kron (*ASP Conf. Ser.*, **10**), in press.
Chambers, K. C., Miley, G. K., and Joyce, R. R. 1988, *Ap. J. (Letters)*, **329**, L75.
Chambers, K. C., Miley, G. K., and van Breugel, W. 1987, *Nature*, **329**, 604.
———. 1988, *Ap. J. (Letters)*, **327**, L47.
———. 1990, in preparation.
Christian, C., Adams, M., Barnes, J., Butcher, H., Hayes, D., Mould, J., and Siegel, M. 1985, *Pub. A.S.P.*, **97**, 363.
Daly, R. 1990, *Ap. J.*, **355**, 416.
Danzinger, I. J., Fosbury, R. A. E., Goss, W. M., Bland, J., and Boksenberg, A. 1984, *M.N.R.A.S.*, **208**, 589.
De Veny, J. 1985, *Observer's Manual for the Cryogenic Camera* (Tucson: Kitt Peak National Observatory).
De Young, D. 1981, *Nature*, **293**, 43.
———. 1986, *Ap. J.*, **307**, 62.
———. 1989, *Ap. J. (Letters)*, **342**, L59.
di Serego Alighieri, S., Fosbury, R. A. E., Tadhunter, C. N., and Quinn, P. J. 1989, *Nature*, **341**, 307.
Djorgovski, S., Spinrad, H., McCarthy, P., Dickinson, M., van Breugel, W., and Strom, R. 1988, *A.J.*, **96**, 836.
Eales, S. A., Alexander, P., and Duncan, W. A. 1990, *M.N.R.A.S.*, **240**, 817.
Eales, S. A., and Rawlings, S. 1990, *M.N.R.A.S.*, **243**, 1P.
Eisenhardt, P., and Chokshi, A. 1990, *Ap. J. (Letters)*, **351**, L9.
Elias, J. H., Frogel, J. A., Matthews, K., and Neugebauer, G. 1982, *A.J.*, **87**, 1029.
Fabian, A. C. 1989, *M.N.R.A.S.*, **238**, 41P.
Fall, S. M., and Rees, M. J. 1985, *Ap. J.*, **298**, 18.
Fanaroff, B. L., and Riley, J. M. 1974, *M.N.R.A.S.*, **167**, 31.
Ferland, G. J., and Netzer, H. 1983, *Ap. J.*, **264**, 105.
Foltz, C., Weymann, R., Hazard, C., and Turnshek, D. 1983, *Pub. A.S.P.*, **95**, 117.
Fosbury, R. A. E., Tadhunter, C. N., and Danzinger, I. J. 1984, *M.N.R.A.S.*, **208**, 955.
Gopal-Krishna. 1988, *Astr. Ap.*, **192**, 903.
Halpern, J. P., and Steiner, J. E. 1983, *Ap. J. (Letters)*, **269**, L37.
Heckman, T. M., Miley, G. K., Balick, B., van Breugel, W. J. M., and Butcher, H. R. 1982, *Ap. J.*, **262**, 529.
Heeschen, D. 1960, *Pub. A.S.P.*, **72**, 368.
Kardeshev, N. S. 1962, *Soviet Astr.*, **6**, 317.
Laing, R. A., and Peacock, J. A. 1980, *M.N.R.A.S.*, **190**, 903.
Laing, R. A., Riley, J. M., and Longair, M. S. 1983, *M.N.R.A.S.*, **204**, 151.
Le Fèvre, O., and Hammer, F. 1988, *Ap. J. (Letters)*, **333**, L37.
Lilly, S. J. 1988, *Ap. J.*, **333**, 161.
———. 1989*a*, private communication.
———. 1989*b*, *Ap. J.*, **340**, 77.
Lilly, S. J., and Longair, M. S. 1984, *M.N.R.A.S.*, **211**, 833.
McCarthy, P. J. 1989, Ph.D. thesis, University of California, Berkeley.
McCarthy, P. J., Spinrad, H., Djorgovski, S., Strauss, M. A., van Breugel, W. J. M., and Liebert, J. 1987*a*, *Ap. J. (Letters)*, **319**, L39.
McCarthy, P. J., van Breugel, W., Spinrad, H., and Djorgovski, S. 1987*b*, *Ap. J. (Letters)*, **321**, L29.
———. 1990, submitted *Ap. J.*,
McLean, I. 1987, in *Infrared Astronomy with Arrays*, ed. C. G. Wynn-Williams and E. E. Beckin (Honolulu: University of Hawaii), p. 180.
Miley, G. K. 1980, *Ann. Rev. Astr. Ap.*, **18**, 165.
Miley, G. K., Heckman, T. M., Butcher, H. R., and van Breugel, W. J. M. 1981, *Ap. J. (Letters)*, **247**, L5.
Osterbrock, D. E. 1989, *Astrophysics of Gaseous Nebulae and Active Galactic Nuclei* (Mill Valley: University Science Books).
Pacholczyk, A. G. 1970, *Radio Astrophysics* (San Francisco: W. H. Freeman).
Pelletier, G., and Roland, J. 1988, *Astr. Ap.*, **196**, 71.
Perley, R. A., Dreher, J. W., and Cowan, J. J. 1984, *Ap. J. (Letters)*, **285**, L35.
Prévot, M. L., Lequeux, J., Maurice, E., Prévot, L., and Rocca-Volmerange, B. 1984, *Astr. Ap.*, **132**, 389.
Rees, M. J. 1989, *M.N.R.A.S.*, **239**, 1P.
Rocca-Volmerange, B. 1989, in *Proc. Teneriffe Conference, Evolutionary Phenomena in Galaxies*, ed. J. Beckman (Cambridge: Cambridge University Press), in press.
Rocca-Volmerange, B., and Guiderdoni, B. 1989, *Proc. Moriond Conference, The Quest of the Cosmological Constants*, in press.
Roland, J., Hanish, R. J., Véron, P., and Fomalont, E. 1985, *Astr. Ap.*, **148**, 323.
Roland, J., Pelletier, G., and Muxlow, T. 1988, *Astr. Ap.*, **207**, 16.
Roland, J., Véron, P., Stannard, D., and Muxlow, T. 1982, *Astr. Ap.*, **116**, 60.
Rudnick, L. 1988, *Ap. J.*, **325**, 189.
Savage, B. D., and Mathis, J. S. 1979, *Ann. Rev. Astr. Ap.*, **17**, 73.
Scalo, J. M. 1986, *Fund. Cosmic Phys.*, **11**, 1.
Scarrott, S. M., Rolph, C. D., and Tadhunter, C. N., 1990, *M.N.R.A.S.*, **243**, 5P.
Scheuer, P. A. G. 1974, *M.N.R.A.S.*, **166**, 513.
———. 1982, in *IAU Symposium 97, Extragalactic Radio Sources*, ed. D. S. Heeschen and C. M. Wade (Dordrecht: Reidel), p. 163.
Schoening, W. 1987, *Observer's Manual for the Prime Focus Camera* (Tucson: Kitt Peak National Observatory).
Spinrad, H. 1986, *Pub. A.S.P.*, **98**, 269.
———. 1989*a*, in *Epoch of Galaxy Formation*, ed. C. S. Frenk (Dordrecht: Kluwer), p. 39.
———. 1989*b*, private communication.
Spinrad, H., and Djorgovski, S. 1987, in *IAU Symposium 123, Observational Cosmology*, ed. G. Burbidge (Dordrecht: Reidel), p. 129.
Spinrad, H., Djorgovski, S., Marr, J., and Aguilar, L. 1985, *Pub. A.S.P.*, **97**, 932.
Steiner, J. E. 1981, *Ap. J.*, **250**, 469.
Tadhunter, C. N., Fosbury, R. A. E., and di Serego Alighieri, S. 1989, *Proc. of the Como Conf. on BL Lac Objects: 10 Years After*, ed. L. Maraschi, in press.
Tielens, A. G., Miley, G. K., and Willis, A. 1979, *Astr. Ap. Suppl.*, **35**, 153.
Unger, S. W., Pelar, A., Axon, D. J., Whittle, M., Meurs, E. J. A., and Ward, M. J. 1987, *M.N.R.A.S.*, **228**, 671.
van Breugel, W. J. M. 1986, *Canadian J. Phys.*, **64**, 392.
van Breugel, W. J. M., Miley, G. K., Heckman, T. M., Butcher, H. R., and Bridle, A. 1985, *Ap. J.*, **290**, 496.

K. C. CHAMBERS and G. K. MILEY: Sterrewacht, Leiden Observatory, Postbus 9513, 2300 RA Leiden, The Netherlands

W. VAN BREUGEL: Institute for Geophysics and Planetary Physics, Lawrence Livermore National Laboratory, P.O. Box 808, L-413, Bldg 319, Livermore, CA 94550

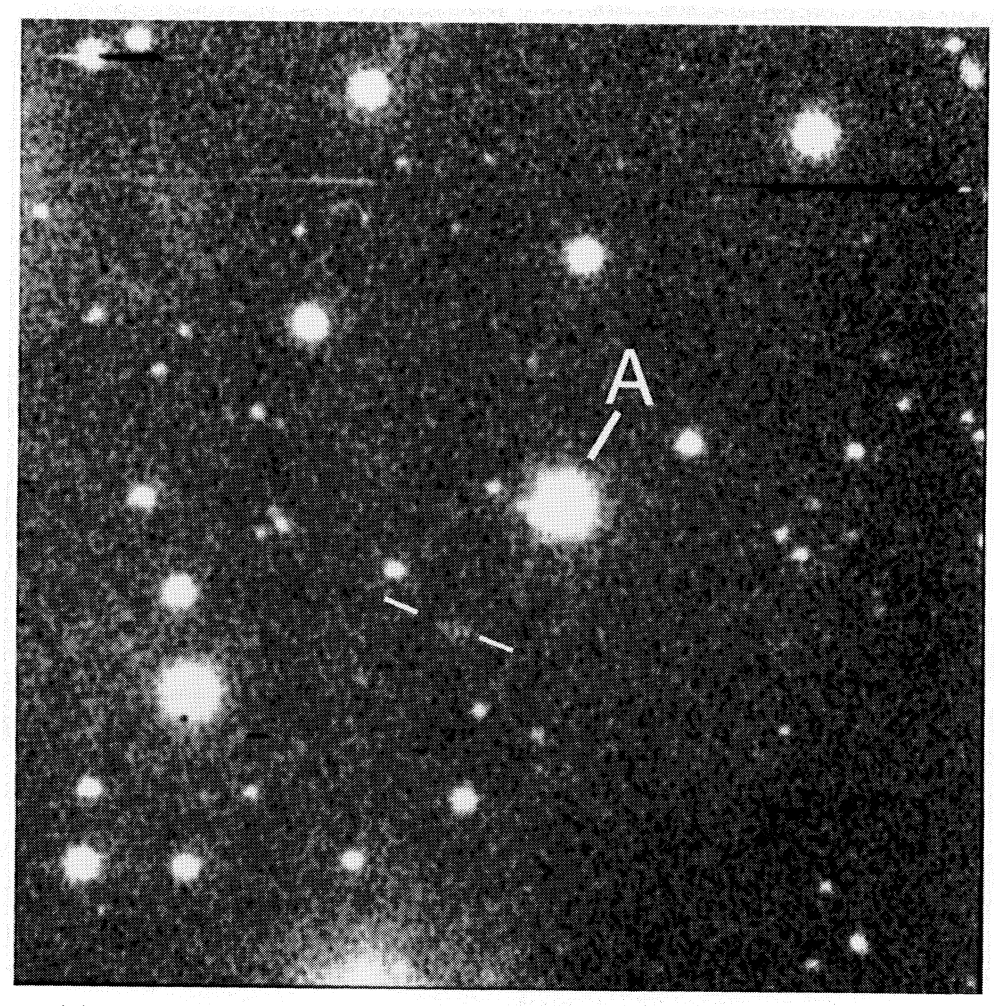

FIG. 1.—Finding chart, consisting of the entire *R* band CCD image ~3'.5 across. North is up, and east is to the left. The object we associate with 4C 41.17 is indicated by the two bars. In the center of the image is marked star "A" which is visible on the Sky Survey and whose (1950) coordinates are in Table 4.

CHAMBERS, MILEY, AND VAN BREUGEL (*see* **363**, 23

PLATE 2

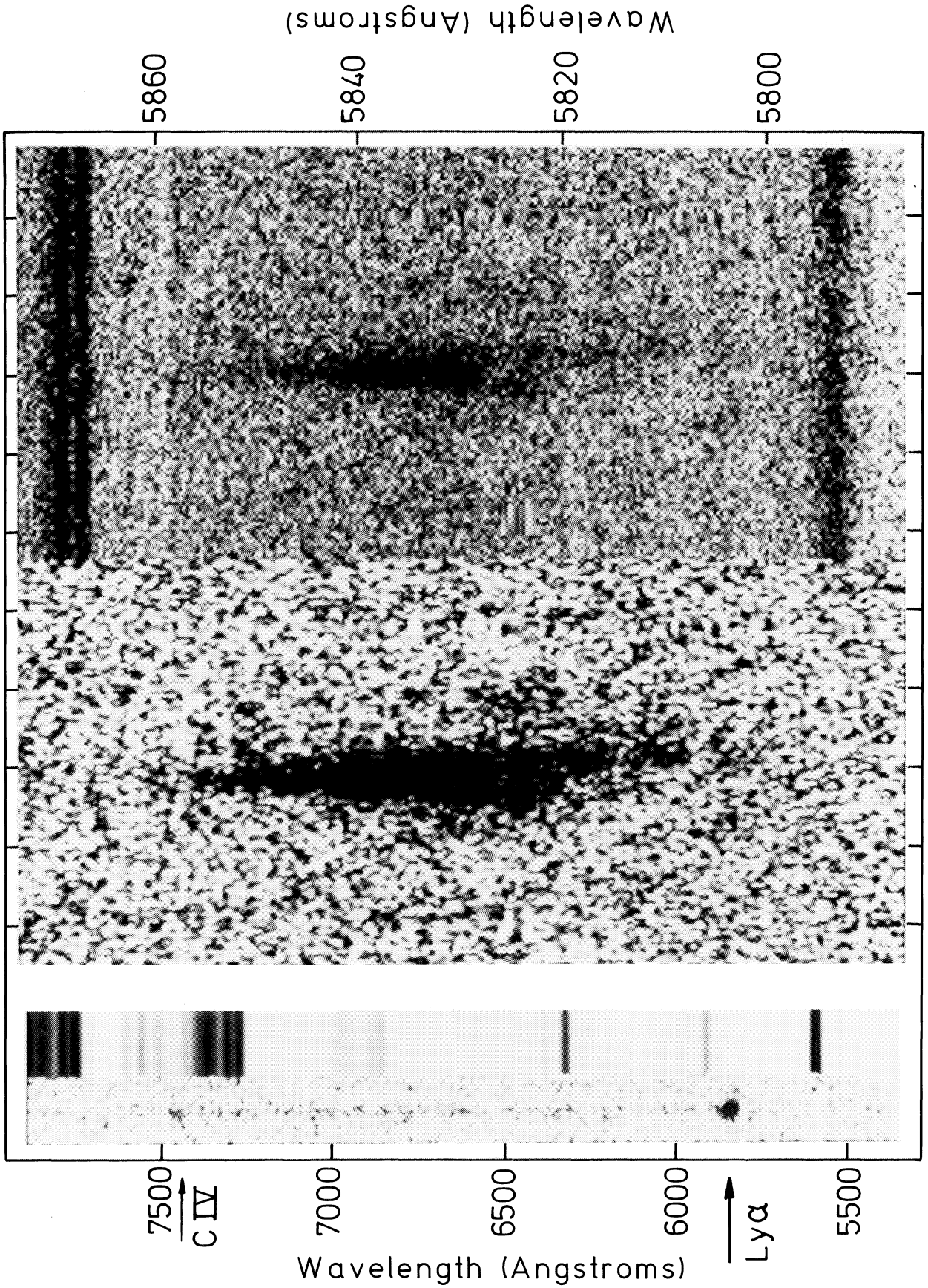

FIG. 2.—(*a*) Sky-subtracted low-dispersion slit spectrogram of 4C 41.17 at PA 70°. (*b*) Unsubtracted spectrogram. (*c*) Sky-subtracted high-dispersion slit spectrogram of Lyα line of 4C 41.17 at PA 70°. (*d*) Unsubtracted spectrogram. Object designated "disk" is most visible in this image.

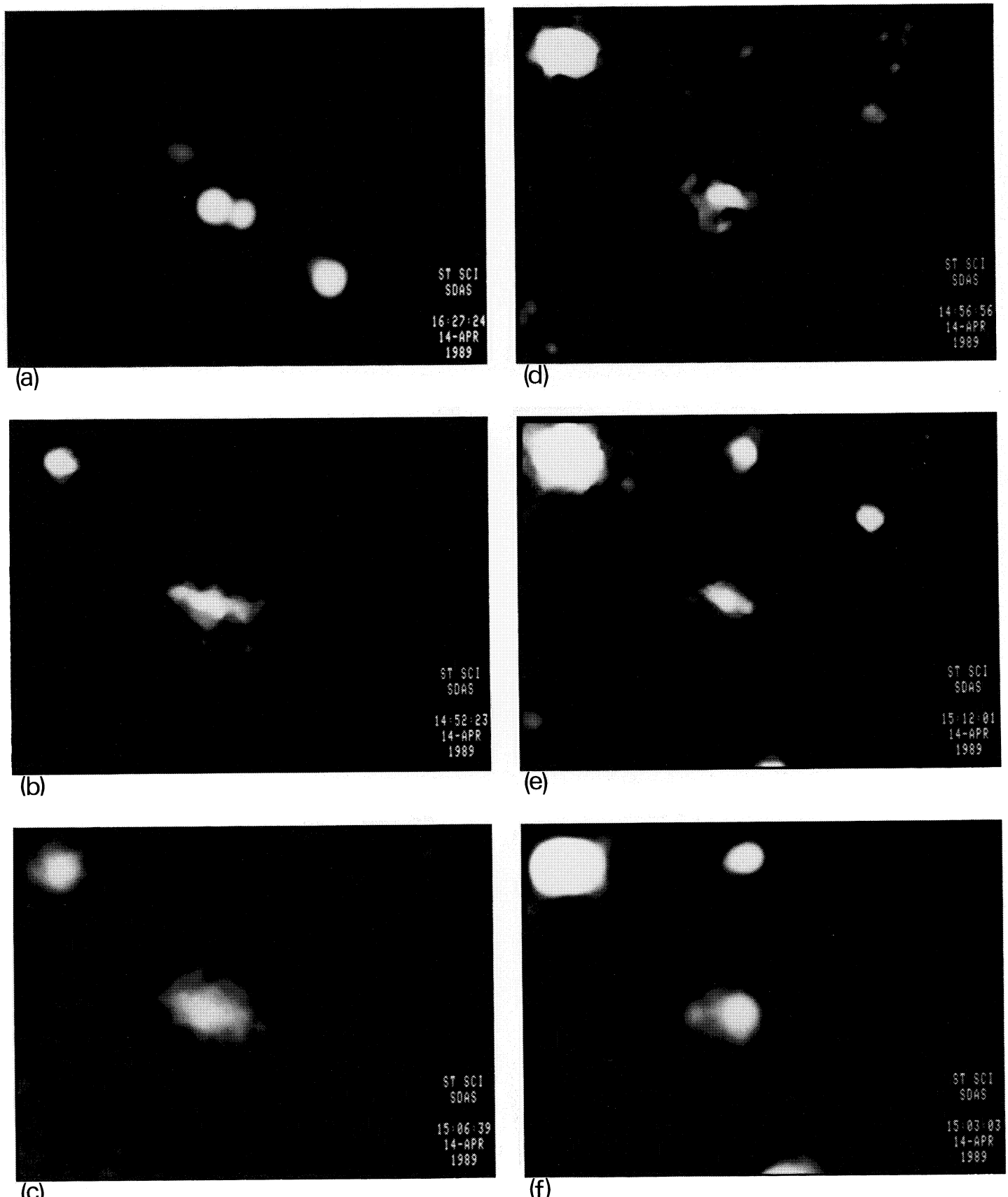

FIG. 6.—Radio, infrared, and optical photographs of 4C 41.17. For details, see the legend to Fig. 3. The total dimension in declination of each is 23".1. Some details of the structures are more apparent in the photographs than in the contour maps. (*a*) VLA 4885 MHz. (*b*) Best seeing Lyα image. (*c*) Smoothed Lyα image. (*d*) *R* band. (*e*) *I* band. (*f*) Smoothed *K* band image.